NASA TECHNICAL NOTE

NASA TN D-5233

C.1

NASA TN D-5233

HYPERSONIC FLUTTER ANALYSIS USING MEASURED STATIC AERODYNAMIC DERIVATIVES, AND COMPARISON WITH EXPERIMENT

by Robert C. Goetz

Langley Research Center
Langley Station, Hampton, Va.

NATIONAL AERONAUTICS AND SPACE ADMINISTRATION • WASHINGTON, D. C. • MAY 1969

HYPERSONIC FLUTTER ANALYSIS USING MEASURED STATIC AERODYNAMIC DERIVATIVES, AND COMPARISON WITH EXPERIMENT

By Robert C. Goetz

Langley Research Center
Langley Station, Hampton, Va.

NATIONAL AERONAUTICS AND SPACE ADMINISTRATION

For sale by the Clearinghouse for Federal Scientific and Technical Information
Springfield, Virginia 22151 – CFSTI price $3.00

HYPERSONIC FLUTTER ANALYSIS USING MEASURED STATIC AERODYNAMIC DERIVATIVES, AND COMPARISON WITH EXPERIMENT

By Robert C. Goetz
Langley Research Center

SUMMARY

A two-part investigation was conducted, the final intent being to evaluate a quasi-steady flutter analysis technique, using measured static aerodynamic derivatives, at hypersonic speeds. In the first part, static force and moment data were obtained for a series of square-planform double-wedge airfoils with both sharp and circularly blunted leading edges. Aerodynamic characteristics were obtained in helium flow over an angle-of-attack range of -2° to 8° at Mach numbers of 6.8 and 15.3. The results indicate that increasing the leading-edge bluntness greatly increases the drag and decreases the lift at a given angle of attack at both Mach numbers. These trends are shown to be in agreement with modified Newtonian theory. However, at a given angle of attack, the increase in lift coefficient between Mach numbers of 6.8 and 15.3 was not adequately predicted by the theory. At a Mach number of 6.8 the aerodynamic center was found to shift forward with increase in bluntness, while at a Mach number of 15.3 there was a slight rearward shift. Newtonian theory predicts a forward shift with increase in bluntness, and in all cases placed the aerodynamic center forward of the experimentally determined locations.

In the second part of the investigation, a two-degree-of-freedom quasi-steady flutter analysis, including rate terms, is formulated for these airfoils in terms of the experimentally determined slope of the lift curve and location of the aerodynamic center. The resulting analytical solutions are evaluated by comparison with existing experimental flutter results. These comparisons indicate that the pitch-rate term (moment due to damping in pitch) has a significant effect upon the flutter solution and should be included in the quasi-steady analysis. And, finally, the comparisons show that the quasi-steady technique, utilizing measured static aerodynamic quantities, is capable of about 95-percent accuracy in predicting flutter at hypersonic speeds.

INTRODUCTION

The aerodynamic theories ordinarily used in hypersonic flutter analyses are piston theory and Newtonian theory; they are easily applied and afford reasonable accuracy for

simple configurations. Both theories are applied to unsteady problems in a quasi-steady approach formulated on the assumption that the aerodynamic forces on an oscillating airfoil may be defined, at any instant of time, as the steady-state aerodynamic forces associated with the instantaneous angle of attack. This approach, which neglects only the influence of the wake vortices on the flow, is appropriate for hypersonic flutter because of the extremely low reduced frequency (due to high flow velocities) of the unsteady motion. However, each theory includes other assumptions that limit its range of applicability.

Piston theory is developed for cases where the product of Mach number and surface inclination is less than 1, and Newtonian theory is applicable for high Mach numbers and large surface inclinations. In addition, these theories neglect viscous effects, which can be significant at hypersonic speeds, and configuration flow-field effects, which can also be significant if the component under study is in a complex local flow field caused by adjacent components. Thus, the flutter analysis of realistic cases by means of these aerodynamic theories would yield questionable results.

A less formal, and more empirical, analysis of realistic flutter cases is the quasi-steady approach using measured static aerodynamic derivatives. These measured quantities reflect the actual pressure distribution of the component under study, thereby including viscous and configuration flow-field effects. Additionally, the range of applicability would include complex configurations and configurations at angles of attack.

The flutter mechanism has been described in terms of simply defined static aerodynamic forces by various investigators in the past, such as Pines (ref. 1) and Bryce et al. (ref. 2). More recently this approach has been utilized to predict flutter on wings at angle of attack in the transonic and supersonic speed ranges (ref. 3).

The present study was undertaken to evaluate the use of measured static aerodynamic derivatives in a quasi-steady flutter analysis at hypersonic speeds. Selected for study were relatively simple rigid models similar to those previously investigated for flutter, experimentally and analytically, at Mach numbers of 6.8 and 15.4 (refs. 4 and 5). These models were square-planform double-wedge airfoils with circular leading and trailing edges.

The investigation was in two parts. In the first part, static aerodynamic data were obtained for the models in helium flow in the Langley Mach 7 and Mach 15 hypersonic aeroelasticity tunnels over an angle-of-attack range from -2° to 8°. The resulting aerodynamic characteristics are compared with those predicted by Newtonian and modified Newtonian theories. In the second part of this report, a two-degree-of-freedom quasi-steady flutter analysis, including rate terms, is formulated for the airfoil configurations in terms of the experimentally determined static aerodynamic characteristics. An explicit solution to the flutter problem is presented, utilizing pitch-rate derivatives which

are assumed to be known, and the flutter characteristics for the model configurations are calculated. These quasi-steady analytical results are compared with existing experimental and analytical flutter results for identical models (refs. 4 and 5). In addition, the present paper contains an evaluation of the effect of pitch rate on flutter, and also quasi-steady flutter results for the same configurations at angles of attack up to 8°.

SYMBOLS

b	wing semichord
C_D	wing drag coefficient
C_L	wing lift coefficient
C_{L_α}	wing lift-curve slope
C_m	wing pitching-moment coefficient
C_p	pressure coefficient
$C_{\Delta p}$	local coefficient of lifting pressure difference (see eq. (5))
$C_{\Delta p_\alpha}$	local lift-curve slope (see eq. (6))
c	wing chord
c_l	section lift coefficient
c_{l_α}	section lift-curve slope, $\partial c_l / \partial \alpha$ (see eq. (7))
h_{pa}	vertical displacement of the pitch axis
k	reduced frequency, $b\omega_f/V$
L	lift
L_i	dimensionless coefficients defining lift on an oscillating wing section ($i = 1, 2, 3, 4$) (see eqs. (11))

M	Mach number
M_i	dimensionless coefficients defining moment on an oscillating wing section ($i = 1, 2, 3, 4$) (see eqs. (11))
M_α	aerodynamic moment on wing section about the pitch axis
p_l	local pressure on lower surface
p_u	local pressure on upper surface
q	dynamic pressure, $\rho V^2/2$
r	radius of leading edge
$\bar{r}$	nondimensional leading-edge radius, r/c
r_α	normalized radius of gyration of wing about pitch axis
s	wing semispan
t	time
V	flow velocity
$\overline{V}$	flutter speed normalized by the flutter speed at a mean angle of attack of 0^o
w	downwash
w_i	component of downwash due to time variation of displacements (eq. (4))
x	chordwise coordinate measured from leading edge (fig. 16)
$\bar{x}$	distance from pitch axis to experimental aerodynamic center, positive aft
x_{ac}	distance from wing leading edge to aerodynamic center
x_{pa}	distance from wing leading edge to pitch axis

$\bar{x}_{pa} = \frac{x_{pa}}{c}$

x_α	dimensionless static unbalance
y	spanwise coordinate measured from root chord (fig. 16)
z	coordinate normal to x and y (fig. 16)
α	local angle of pitch of airfoil (geometric angle of attack since wing is rigid in camber) (see fig. 16)
α_i	perturbation pitch angle
α_m	mean angle of attack
γ	ratio of specific heats, 5/3 for helium
δ	wedge half-angle
μ	mass ratio (ratio of mass of wing to mass of test medium contained in volume generated by revolving each streamwise chord about its midpoint)
ρ	density of test medium
$\bar{\tau}$	maximum ratio of airfoil thickness to chord
$\bar{\tau}_{te}$	ratio of thickness to chord at wing trailing edge
ω_f	flutter frequency
ω_h	frequency of uncoupled plunging mode
ω_i	natural frequency of ith mode (i = 1, 2, 3, . . .)
ω_α	frequency of uncoupled pitching mode

Subscripts:

exp	experimental

stag stagnation

th theoretical

Dots over symbols denote differentiation with respect to time.

STATIC AERODYNAMIC CHARACTERISTICS

Apparatus and Models

The tests were conducted in the Langley hypersonic aeroelasticity tunnels (HAT). This facility uses helium as a test medium and is of the blowdown type. At the time of the investigation it had two contoured nozzles designed to generate uniform flows at Mach numbers of 6.8 and 15.3. A description of the $M = 6.8$ leg is given in reference 6, and a description of the $M = 15.3$ leg is presented in reference 5.

Two series of airfoil models were tested, each having semispan aspect ratios of 1.0, zero sweep, and no taper. The basic model had a double-wedge profile with a wedge half-angle of 5° and the maximum thickness at the midchord, and was geometrically identical to the flutter models of references 4 and 5. Each series consisted of three basic models with leading-edge radii of 0, 3, and 6 percent of their chord. The difference between the two series was that the one tested at $M = 15.3$ had a 6-inch (15.24-cm) chord, whereas the one tested at $M = 6.8$ had a 4-inch (10.16-cm) chord. The latter series of models is shown in figure 1.

All the models were accurately machined from solid steel and were highly polished. The surfaces and edges were maintained in good condition during the tests by periodic polishing. For aerodynamic-data acquisition they were mounted on strain-gage balances, as shown in figure 2, which were integral with supporting shafts that were in turn clamped to the side wall of the wind tunnel.

The models were separated from the tunnel-wall boundary layer during the tests by reflection-plane systems identical to those used in references 4 and 5. The arrangement of one of the models and the reflection-plane system in the Mach 15.3 leg of the HAT facility is shown in figures 3(a) and 3(b).

Test Procedure

For each test run the models were positioned on the reflection plane at the desired angle of attack with respect to the free-stream flow, the angle of attack ranging from -2° to 8°. This preset angle of attack was monitored during the test run by means of high-speed motion pictures. For the tests at $M = 15.3$ the models were protected from the

starting and stopping transients of the tunnel flow by a cover wedge, shown extended in figure 3(c), which was retracted to a position between the reflection plane and the tunnel side wall, as illustrated in figure 3(b), during the data-acquisition portion of the run. For the tests at $M = 6.8$ the models and their support structures were initially positioned in an enclosure immediately adjacent to, but outside of, the test section and were injected into the test section subsequent to passage of the flow starting transient, and then retracted prior to the flow stopping transient. These procedures were necessary in order to protect the sensitive strain-gage balance from the high loads associated with the starting and stopping transients.

The operating procedure was similar for both series of models. After a model was installed, the tunnel was evacuated to a low pressure. A control valve upstream of the test section was opened and flow was established at a constant Mach number and a low dynamic pressure. At this time the model was exposed to the flow by one of the two methods previously described, and the dynamic pressure was increased slowly to the desired value. Then the model was again protected and the flow stopped. Throughout the tunnel operation, stagnation temperatures and pressures were recorded on an oscillograph together with signals from the six components of the strain-gage balance, so that tunnel conditions could be correlated with the model force and moment data.

Results and Discussion

Complete force and moment data were obtained for the various airfoil configurations at the same test conditions as were used in the flutter tests of references 4 and 5, namely, nominal Mach numbers of 6.8 and 15.3 and Reynolds numbers based on the wing chord of 4.8×10^6 and 2.4×10^6, respectively. The coefficients of lift, drag, and pitching moment about two axes are presented as a function of angle of attack at each test Mach number in figures 4 to 9 and the trends are illustrated by faired lines through the experimental data. The aerodynamic coefficients were reduced from the measured data, after the measured data had been corrected in the usual manner for balance component-interaction effects. In the data reduction, the planform area and wing-chord length were used for reference.

Shown collected in figures 10(a) and 10(b) are the faired experimental lift-coefficient data for each of the three airfoil configurations at each Mach number, presented as a function of angle of attack. Increasing the leading-edge bluntness is shown to decrease the airfoil lift coefficient for a given angle of attack at both Mach numbers. However, for a given amount of leading-edge bluntness the lift coefficient is higher at $M = 15.3$ (fig. 10(b)) than at $M = 6.8$ (fig. 10(a)) over the entire angle-of-attack range of the tests. Included in figure 10 are theoretical lift-coefficient values obtained from modified Newtonian theory $\left(C_p = C_{p,stag} \sin^2\phi\right.$, where ϕ is the angle between the flow and a

tangent to the exposed surface). While the trends of decreasing lift coefficient with increasing bluntness are predicted at both Mach numbers, the theory predicts only slightly higher absolute values at the higher Mach number for a given configuration. Consequently, modified Newtonian theory compares well with the measured results at $M = 6.8$, but is quite low at $M = 15.3$. Additionally, even unmodified Newtonian theory predictions (not shown) are lower than the experimental values at $M = 15.3$. However, it should be noted that the theory does not account for the viscous effects which would be reflected in the test results. At hypersonic speeds the boundary layers at a given Reynolds number are thicker than those at lower speeds. This thickening of the boundary layer in effect increases the wedge angle, thus resulting in higher surface pressures than predicted by inviscid-flow theories.

The drag coefficient at a mean angle of attack of 0° is presented in figure 11 as a function of leading-edge radius. A great increase in drag with increased bluntness is illustrated; the drag loading is increased by about a factor of 20 when a sharp leading edge is replaced by one with a radius equal to 6 percent of the airfoil chord. Newtonian theory is shown to be inaccurate for the sharp configuration, and although much better for the blunt models, it is about 10 percent lower than the test results for $M = 15.3$ and about 20 percent higher than the test results for $M = 6.8$.

From the wind-tunnel static measurements presented in figures 4 to 9, faired values of the slope of the lift curve C_{L_α} and location of the aerodynamic center x_{ac} can be obtained. Values of these two quantities for the series of airfoils of this investigation are presented as a function of angle of attack in figures 12 and 13. These quantities reflect the effects of the blunt leading edge and the boundary layer on the pressure distribution. The results indicate that at both Mach numbers the slope of the lift curve decreases with increase in leading-edge bluntness. At $M = 6.8$ the aerodynamic center shifts forward with increasing bluntness, while at $M = 15.3$ it shifts slightly rearward with increasing bluntness. There is also the expected rearward shift of the aerodynamic center with increase in angle of attack for all configurations at both Mach numbers.

In figure 14 the lift-curve slope at $\alpha_m = 2^{\circ}$ is presented as a function of leading-edge radius. Included for comparison are the theoretical values predicted by Newtonian and modified Newtonian theory. The experimental aerodynamic centers for $\alpha_m = 2^{\circ}$, as well as Newtonian predictions, for the series of airfoils at both Mach numbers are presented in figure 15. Newtonian theory predicts a forward shift of the aerodynamic center with increase in bluntness, which is in agreement with the $M = 6.8$ test results. However, in all cases Newtonian theory placed the aerodynamic center forward of the experimentally determined locations. This is probably because the theoretical treatment

assumes that no lift is generated aft of the midchord of the double-wedge configuration, that is, in the region in the aerodynamic "shadow."

HYPERSONIC QUASI-STEADY FLUTTER ANALYSIS AND COMPARISON WITH EXPERIMENT

Analysis

A rigid airfoil section of unit width, of the configuration shown in figure 16 (with a right-hand coordinate system x,y,z), is considered to be oscillating about the pitch axis and plunging. The section has an angular displacement α and a vertical displacement at the pitch axis h_{pa}. The angular displacement is represented as

$$\alpha \equiv \alpha(t) = \alpha_m + \alpha_i(t) \tag{1}$$

where α_m is a mean angle about which a perturbation $\alpha_i(t)$ can take place. Let the shape of the airfoil section be represented by $Z_S \equiv Z_S(x)$ where Z_S is positive outward from the midplane for both surfaces. Thus the z-coordinate of the airfoil surface for time-varying displacements is, for small α,

$$z = z(x,t) = -h_{pa}(t) \pm Z_S(x) - (x - x_{pa})\alpha(t) \tag{2}$$

where the upper and lower of the signs with $Z_S(x)$ apply to the upper and lower surfaces, respectively, of the airfoil.

The total downwash ratio (positive down) at the airfoil surface is

$$\frac{w}{V} = -\frac{1}{V}\left(\frac{d}{dt} + V\frac{d}{dx}\right)z = \left[\mp\frac{dZ_S(x)}{dx} + \alpha_m\right] + \frac{1}{V}\left[\dot{h}_{pa} + (x - x_{pa})\dot{\alpha}_i + V\alpha_i\right] \tag{3}$$

The part of the downwash ratio that is due to the time variation of h_{pa} and α is the last three terms, or

$$\frac{w_i}{V} = \frac{\dot{h}_{pa}}{V} + \frac{x - x_{pa}}{V}\dot{\alpha}_i + \alpha_i \tag{4}$$

The coefficient of lifting pressure difference at a point x on the chord is denoted by

$$C_{\Delta p} = C_{\Delta p}(x) = \frac{p_l(x) - p_u(x)}{q} \tag{5}$$

For use in a linear-type analysis the local lift-curve slope is

$$\frac{\partial}{\partial\alpha} C_{\Delta p}(x) = C_{\Delta p_\alpha}(x) \tag{6}$$

where the angle α itself is a function of x and for the present analysis, as in reference 7, is taken to be equal to w_i/V of equation (4) for the small deflections being considered. Inherent in this equivalence is the usual assumption made for high speeds and slow oscillations (low reduced frequency k) that a point-function relationship exists between the local pressure difference on the surface of a wing and the normal component of fluid velocity produced by the wing's motion. Also, as in reference 7, the section value c_{l_α} is defined as

$$c_{l_\alpha} = \frac{1}{c}\int_0^c C_{\Delta p_\alpha}(x)dx \tag{7}$$

The quasi-steady lift (positive down, as in much of the flutter literature) can then be expressed as

$$-L = \int_0^c C_{\Delta p_\alpha} q \frac{w_i(x)}{V} dx = \int_0^c C_{\Delta p_\alpha} q \left[\alpha_i + \frac{\dot{h}_{pa}}{V} + (x - x_{pa})\frac{\dot{\alpha}_i}{V}\right]dx \tag{8}$$

As in reference 7, the distance from the pitch axis to the section aerodynamic center, whether obtained experimentally or analytically, is defined as

$$\bar{x} = \frac{\int_0^c C_{\Delta p_\alpha}(x - x_{pa})dx}{\int_0^c C_{\Delta p_\alpha} dx} \tag{9}$$

By use of equations (7) and (9) in equation (8), the quasi-steady section lift can be expressed as

$$-L = qcc_{l_\alpha}\left(\alpha_i + \frac{\dot{h}_{pa}}{V} + \frac{\bar{x}\dot{\alpha}_i}{V}\right) \tag{10a}$$

A parallel development gives the quasi-steady section pitching moment as

$$-M_\alpha = qc\left[c_{l_\alpha}\bar{x}\left(\alpha_i + \frac{\dot{h}_{pa}}{V}\right) + \frac{\dot{\alpha}_i}{cV}\int_0^c C_{\Delta p_\alpha}(x - x_{pa})^2 dx\right] \tag{10b}$$

For simple harmonic motion the section lift and moment can be expressed in terms of the complex coefficient form of Garrick and Rubinow (ref. 8) as

$$\left.\begin{aligned} -L &= 4\rho bV^2k^2\left[(L_1 + iL_2)\frac{h_{pa}}{b} + (L_3 + iL_4)\alpha_i\right] \\ -M_\alpha &= 4\rho b^2V^2k^2\left[(M_1 + iM_2)\frac{h_{pa}}{b} + (M_3 + iM_4)\alpha_i\right] \end{aligned}\right\} \tag{11}$$

Before relating the coefficients of equations (10a) and (10b) to those of equations (11), the application of the experimentally measured static aerodynamic derivative C_{L_α} is

described as follows. In the experimental program described in the section entitled "Static Aerodynamic Characteristics" the aerodynamic derivatives were measured for the whole model rather than for any section. However, the model was unswept and its geometry was uniform in the spanwise direction. Therefore, the section properties c_{l_α} and $\bar{x}$ are considered to have the same numerical values as C_{L_α} and $\bar{x}$ for the whole wing. With this consideration, the relationships between the coefficients are

$$\left.\begin{aligned} L_1 &= 0 & M_1 &= 0 \\ L_2 &= \frac{C_{L_\alpha}}{4k} & M_2 &= \frac{C_{L_\alpha}}{4k}\frac{\bar{x}}{b} \\ L_3 &= \frac{C_{L_\alpha}}{4k^2} & M_3 &= \frac{C_{L_\alpha}}{4k^2}\frac{\bar{x}}{b} \\ L_4 &= \frac{C_{L_\alpha}}{4k}\frac{\bar{x}}{b} & M_4 &= \int_0^c \frac{C_{\Delta p_\alpha}(x - x_{pa})^2}{kc^3}\,dx \end{aligned}\right\} \tag{12}$$

It can be seen from equations (11) and (12) that all the oscillatory forces necessary for a flutter analysis can be expressed in terms of experimentally determined values of the lift-curve slope and the location of the aerodynamic center relative to the axis of rotation, except M_4, the moment due to damping in pitch. For the purposes of this investigation M_4 is represented by expressions derived from piston theory and Newtonian theory at $M = 6.8$ and 15.3, respectively.

The piston-theory expression for M_4 taken directly from reference 9, for the second-order expansion of the downwash, is

$$M_4 = \frac{1}{Mk}\frac{4}{3} + \frac{\gamma + 1}{k}\left(\bar{\tau}_{te} - 2\frac{M_{w_1}}{c^3}\right) - 2\bar{x}_{pa}\left(M_2 + L_4 + 2\bar{x}_{pa}L_2\right) \tag{13}$$

where for a double-wedge airfoil the thickness of the trailing edge $\bar{\tau}_{te}$ is equal to zero, and the first moment of the area of the cross section about the airfoil leading edge in nondimensional form M_{w_1}/c^3 is equal to $\bar{\tau}/4$. Therefore, equation (13) for a double-wedge airfoil reduces to

$$M_4 = \frac{1}{Mk}\frac{4}{3} + \frac{\gamma + 1}{k}\left(-\frac{\bar{\tau}}{2}\right) - 2\bar{x}_{pa}\left(M_2 + L_4 + 2\bar{x}_{pa}L_2\right) \tag{14}$$

It is noted that while equation (14) is derived from piston theory, this expression for M_4 is dependent on oscillatory coefficients $(L_i$ and $M_i)$ which can be expressed in quasi-steady form according to equations (12).

The corresponding expression for a double-wedge airfoil derived from Newtonian theory is obtained from reference 10 as

$$M_4 = \frac{8}{k}\left\{\bar{r}^3\left(\frac{7}{15} - \frac{\pi}{8}\right) + \bar{r}^2\bar{x}_{pa}\left(\frac{\pi}{8} - \frac{2}{3}\right) + \frac{\bar{r}\bar{x}_{pa}^2}{3}\right.$$

$$\left. + \frac{\frac{1 - 2\bar{r}}{\bar{\tau} - 2\bar{r}}}{1 + \left(\frac{1 - 2\bar{r}}{\bar{\tau} - 2\bar{r}}\right)^2}\left[\frac{1}{24} - \frac{\bar{r}^3}{3} - \bar{x}_{pa}\left(\frac{1}{4} - \bar{r}^2\right) + \bar{x}_{pa}^2\left(\frac{1}{2} - \bar{r}\right)\right]\right\} \qquad (15)$$

This Newtonian theory expression for M_4, while not in terms of measured static aerodynamic derivatives, does account analytically for the blunt leading edge which piston theory neglects.

The equations of motion of the airfoil in terms of the two uncoupled degrees of freedom (vertical translation and pitch) lead to the flutter determinant as expressed in reference 8, which is

$$\begin{bmatrix} \left\{\mu\left[\left(\frac{\omega_h}{\omega_f}\right)^2 - 1\right] + L_1 + iL_2\right\}I_1 & \left\{-2\mu x_\alpha + L_3 + iL_4\right\}I_3 \\ \left\{-2\mu x_\alpha + M_1 + iM_2\right\}I_3 & \left\{\mu r_\alpha^2\left[\left(\frac{\omega_\alpha}{\omega_h}\right)^2 - 1\right] + M_3 + iM_4\right\}I_2 \end{bmatrix} = 0 \qquad (16)$$

where

$$I_1 = \int_0^1 \left[h_{pa}\left(\frac{y}{s}\right)\right]^2 d\left(\frac{y}{s}\right)$$

$$I_2 = \int_0^1 \left[\alpha\left(\frac{y}{s}\right)\right]^2 d\left(\frac{y}{s}\right)$$

$$I_3 = \int_0^1 h_{pa}\left(\frac{y}{s}\right)\alpha\left(\frac{y}{s}\right) d\left(\frac{y}{s}\right)$$

and these I_i's allow for spanwise variations of the mode shapes. Expanding equation (16) yields two equations (real and imaginary) which can be solved explicitly for the unknown flutter speed and frequency.

Flutter Experiment

The results of wind-tunnel flutter tests of the model configurations analyzed in the present study are documented in references 4 and 5. The models were tested at a mean angle of attack of 0° and $M = 6.8$ and 15.3 in the Langley hypersonic aeroelasticity tunnels. In these tests the rigid planform was mounted on a flexible shaft; the pitch axis was located at 35 percent of the chord, and the center of gravity was at about 53-percent chord and 50-percent span. The series of flutter models had their leading and trailing edges circularly blunted with radii of 0, 3, and 6 percent of their chord (the same as the aerodynamic-characteristics models) and, additionally, included a model with 1-percent bluntness. Figure 16 illustrates and defines the basic geometric parameters, and details of individual model characteristics are tabulated in references 4 and 5.

Results and Discussion

Equations (12) show that the oscillatory aerodynamic coefficients (except M_4) can be defined in terms of the experimentally determined lift-curve slope and aerodynamic-center location. Utilizing the values given in figures 12 and 13 for these quantities, and the measured mode shapes of references 4 and 5, the flutter condition was determined by solving the resulting equations of the expanded flutter determinant (eq. (16)). Preliminary to achieving an explicit solution, values of M_4 were determined from expressions derived from second-order piston and Newtonian theories (eqs. (14) and (15)) for the $M = 6.8$ and 15.3 cases, respectively. Resulting values of the oscillatory coefficients determined by using the measured static aerodynamic derivatives, and the moments due to damping in pitch (M_4) as determined from equations (14) and (15), are given in table I for the models under consideration. Also included in table I are the resulting calculated values of the flutter velocity and frequency.

These analytical quasi-steady flutter results are presented in figures 17(a) and 17(b) in the form of the flutter velocity-index parameter $V/b\omega_2\sqrt{\mu}$ as a function of leading-edge radius at $M = 6.8$ and 15.3. Also included for comparison are the experimental flutter results of references 4 and 5.

In figure 17(a) the analytical flutter stability boundary, depicted by the dashed curve, predicts the experimental trend of a higher flutter stability boundary with increased bluntness. Examination of the calculated flutter velocity-index values for the configurations tested at $M = 6.8$ having blunt leading edges shows that they compare well with the measured values. However, a variance between the quasi-steady analytical and experimental flutter velocity-index results of about 20 percent is shown to occur for the sharp configuration.

The flutter velocity results for $M = 15.3$ are given in figure 17(b). Again the quasi-steady analytical results are depicted by the dashed curve and they indicate a

higher flutter stability boundary with increase in leading-edge bluntness. A comparison between the calculated and measured flutter velocity-index values shows good agreement for the sharp and 3-percent blunt configurations, but a difference of about 15 percent for the 1-percent blunt configuration.

The results for the 6-percent blunt configuration warrant further discussion. In figure 17 no experimental flutter-velocity data are shown for the 6-percent blunt configuration because the model encountered a static divergence instability at a lower velocity than its flutter boundary. Conventional divergence analysis, wherein the aerodynamic pitching moments reach a value exceeding the torsional rigidity of the airfoil and cause it to diverge statically in the pitch mode, failed to predict this result. However, a newly recognized form of divergence in which drag loading is a significant factor and which is characterized by a mode of deflection consisting of lateral bending (vertical and spanwise displacements) accompanied by pitching is discussed in reference 11 for models supported on long, thin, rectangular shafts. Results of this form of divergence analysis for the 3- and 6-percent blunt configurations are shown by the solid curves in figures 17(a) and 17(b). The details of these calculations are given in reference 11; it is sufficient to mention here that they were made by using measured static aerodynamic quantities, and the resulting divergence instability was dependent upon a combination of the high drag loading and the particular model support arrangement. The agreement between the experimental and calculated divergence results for the 6-percent blunt model is seen to be excellent. Also, the divergence instability is predicted to occur at a higher velocity than the flutter instability for the 3-percent blunt model, a result consistent with the experiment. It should be noted that, like conventional flutter analyses, the quasi-steady flutter analysis as presented herein does not include drag loading or its associated in-plane degree of freedom.

For completeness, figure 18 presents ratios of the experimental to quasi-steady values of the flutter frequency as a function of leading-edge radius. The agreement between the calculated and experimental results is rather poor. This poor agreement is, however, of about the same quality as that obtained from the piston and Newtonian theory calculations of references 4 and 5, and in general is consistent with the findings of other quasi-steady investigations; for example, references 3 and 12.

As was mentioned previously, M_4, the coefficient for damping in pitch, was the only oscillatory aerodynamic coefficient that could not explicitly be expressed in terms of the measured static aerodynamic parameters. Therefore, M_4 was determined from expressions derived from piston and Newtonian theories for the calculations at Mach numbers of 6.8 and 15.3, respectively. Consequently, a parametric study was made to determine the effect of M_4 on the final quasi-steady flutter solution. Results of this study

are presented in figure 19, where the ratio of experimental to theoretical flutter velocities at $M = 15.3$ is shown as a function of the product kM_4. In contrast to the findings of other investigators, notably those of references 7 and 12, the effect of M_4 (at least for these particular configurations at $M = 15.3$) is shown to be appreciable. Increasing the value of kM_4, for example, from 0 to 0.10 increased the quasi-steady flutter velocity by about 20 percent for the sharp airfoil (fig. 19(a)), and about 22 percent for the 3-percent blunt configuration (fig. 19(b)). The values of kM_4 predicted by using Newtonian theory are indicated in the figure and they yield quasi-steady flutter-velocity values 7-percent lower and 3-percent higher than the experimental results for the sharp and 3-percent blunt configurations, respectively.

While the simple configurations of this study are well suited for an exploratory inquiry concerning the empirical quasi-steady flutter technique at high speeds, it is recognized that existing flutter theories can predict their behavior with reasonable accuracy. More specifically, the present flutter velocity and frequency results determined by using the empirical quasi-steady technique reported herein are no better than the piston or Newtonian theory results of references 4 and 5, and for some configurations not quite as good. As an illustration, the flutter velocity and frequency results of reference 5 are compared with the present empirical quasi-steady results for $M = 15.3$ in figure 20. It can be seen that for the slender, sharp, double-wedge configuration the easily applied piston theory offers the best results. But it is emphasized that the potential value of the empirical approach is in the prediction of pitching-plunging flutter conditions for more complicated configurations for which piston and Newtonian theories are not intended to apply. Such configurations include those that have a highly complex flow field over the airfoil, those for which viscous effects should be taken into account, and complex configurations at angle of attack.

A quasi-steady parametric study was conducted for the series of models of this investigation at $M = 15.3$, with initial angle of attack as the isolated parameter. The measured values of the slope of the lift curve and location of the aerodynamic center obtained from figures 12 and 13 were used in equations (12) to find the aerodynamic coefficients. The expression for M_4 was obtained from reference 9, based on the third-order expansion of the downwash to account for contributions due to mean angle of attack. The calculated results are presented in figure 21 in the form of the quasi-steady flutter velocity at angle of attack normalized by the comparable value at zero angle of attack. The results for the sharp and the 3-percent blunt configurations indicate that increasing the angle of attack is destabilizing for the sharp configuration and, to a lesser degree, for the 3-percent blunt configuration. For the 6-percent blunt configuration there seems to be no decrease in stability (in fact, a slight increase for small values of α_m) until the angle of attack reaches 7^o. These results cannot be verified at present because of the

lack of any experimental data for these configurations at angle of attack; however, they are presented to illustrate one possible application of the empirical quasi-steady flutter analysis.

CONCLUSIONS

A quasi-steady flutter analysis, using measured static aerodynamic derivatives for a series of square-planform, 5^{o} half-angle, double-wedge airfoils with both sharp and blunt leading edges, has been made for Mach numbers M of 6.8 and 15.3. Results from experimental programs for measuring the static aerodynamic characteristics and for determining the flutter characteristics, including theoretical-experimental comparisons, lead to the following conclusions:

1. Measured trends of decreasing lift coefficient with increasing bluntness at a given angle of attack α_m (for $0 \leqq \alpha_m \leqq 8^{o}$) are consistent with predictions of modified Newtonian theory. However, the increases in lift with increase in Mach number from 6.8 to 15.3 are not adequately predicted.

2. The drag coefficient for zero lift is seen to increase linearly by a factor of about 20 when the sharp leading edge is replaced by one with a radius equal to 6 percent of the airfoil chord. Newtonian theory drag predictions are inaccurate for the sharp model, but for the blunt configurations they are within 10 percent at $M = 15.3$ and 20 percent at $M = 6.8$.

3. At $M = 6.8$ the aerodynamic center shifts forward with increase in bluntness, while at $M = 15.3$ there is a slight rearward shift. At both Mach numbers the aerodynamic center shifts rearward for all configurations with increase in angle of attack. Newtonian theory predicts, in contrast, a forward shift of the aerodynamic center with increase in bluntness, and in all cases located the aerodynamic center forward of the measured position.

4. Comparing the empirical quasi-steady flutter results with previously reported experimental results indicated agreement within about 5 percent, in predicting flutter speeds, except for the sharp configuration at $M = 6.8$, where the theory was about 20 percent high.

5. At $M = 15.3$, variation of the coefficient of damping in pitch had an appreciable effect upon the quasi-steady flutter results. For example, neglecting this term would cause the flutter velocity to change by about 15 percent for the sharp configuration.

6. Quasi-steady flutter results for the sharp and 3-percent blunt configurations indicate that increasing the mean angle of attack from 0^{o} is mildly destabilizing, but to a

lesser degree for the blunt airfoil. Results for the 6-percent blunt airfoil indicate no similar decrease in stability until the angle of attack reaches 7°.

7. The quasi-steady flutter analysis including pitch-rate terms and utilizing measured static aerodynamic derivatives is capable of considerable accuracy. This technique has potential value for complex configurations including those where viscous and local flow-field effects need to be taken into account.

Langley Research Center,
National Aeronautics and Space Administration,
Langley Station, Hampton, Va., March 20, 1969,
126-14-02-08-23.

REFERENCES

1. Pines, Samuel: An Elementary Explanation of the Flutter Mechanism. Proc. Nat. Specialists Meeting on Dynamics and Aeroelasticity (Fort Worth, Texas), Inst. Aero. Sci., Nov. 1958, pp. 52-58.

2. Bryce, William W.; Cooper, Robert E.; and Gravitz, Sidney I.: Development of a Quasi-Steady Flutter Approach and Correlation of Quasi-Steady, Quasi-Unsteady, and Kernel Function Flutter Analyses With Experimental Data. WADD Tech. Rep. 60-367, U.S. Air Force, May 1960.

3. Brown, D. A.: Flutter Model Tests of Advanced Wing Configurations at Initial Angles of Attack. ASD-TDR-62-498, U.S. Air Force, Oct. 1964.

4. Hanson, Perry W.: Aerodynamic Effects of Some Configuration Variables on the Aeroelastic Characteristics of Lifting Surfaces at Mach Numbers From 0.7 to 6.86. NASA TN D-984, 1961.

5. Goetz, Robert C.: Effects of Leading-Edge Bluntness on Flutter Characteristics of Some Square-Planform Double-Wedge Airfoils at a Mach Number of 15.4. NASA TN D-1487, 1962.

6. Lauten, William T., Jr.; Levey, Gilbert M.; and Armstrong, William O.: Investigation of an All-Movable Control Surface at a Mach Number of 6.86 for Possible Flutter. NACA RM L58B27, 1958.

7. Hall, B. M.; and Martin, E. N.: Theory vs. Test for Hypersonic Flutter Model. Rep. SM-48982, Missile & Space Syst. Div., Douglas Aircraft Co., Inc., Sept. 1965.

8. Garrick, I. E.; and Rubinow, S. I.: Flutter and Oscillating Air-Force Calculations for an Airfoil in a Two-Dimensional Supersonic Flow. NACA Rep. 846, 1946. (Supersedes NACA TN 1158.)

9. Chawla, Jagannath P.: Aeroelastic Instability at High Mach Number. Jour. Aero. Sci., vol. 25, no. 4, April 1958, pp. 246-258.

10. Goetz, Robert C.: Effects of Leading-Edge Sweep on Flutter Characteristics of Some Delta-Planform Surfaces at a Mach Number of 15.4. NASA TN D-2360, 1964.

11. Goetz, Robert C.: Divergence of Some All-Movable Control Surfaces Including Drag Loadings. NASA TN D-4793, 1968.

12. Hurley, S. R.: Hypersonic Flutter Model Tests of Advanced Wing Configurations at Initial Angles of Attack. RTD-TDR-63-4219, U.S. Air Force, Oct. 1964. (Available from DDC as AD 355284.)

TABLE I.- QUASI-STEADY ANALYTICAL FLUTTER RESULTS

$[\gamma = 5/3; \quad \bar{x}_{pa} = 0.35; \quad \alpha_m = 0^o]$

Model[a]	kL_2	k^2L_3	kL_4	kM_2	k^2M_3	kM_4	1/k	$\frac{1/\omega_f,}{\frac{1}{rad/sec}}$	V		$\frac{V}{b\omega_2\sqrt{\mu}}$
									ft/sec	m/sec	
M = 6.8											
0-9-33-2	0.1413	0.1413	-0.00989	-0.00989	-0.00989	0.02068	185	0.00467	6615	2016	1.684
0-9-47-2							109	.00261	6966	2123	1.694
0-9-65-5							66	.00160	6886	2099	1.696
3-14-33-1	.1350	.1350	-.01755	-.01755	-.01755	.03449	158	.00466	5666	1727	1.783
3-14-47-1							109	.00293	6182	1884	1.801
6-20-47-2	.1312	.1312	-.02625	-.02625	-.02625	.04853	148	.00331	7452	2271	1.856
M = 15.3											
0-A-6-1	0.1850	0.1850	-0.01295	-0.01295	-0.01295	0.01112	237	0.00986	6016	1834	1.409
3-A-6-1	.1791	.1791	-.00894	-.00894	-.00894	.01784	262	.00965	6780	2067	1.447
3-A-6-2							250	.00964	6482	1976	1.447
6-A-6-1	.1600	.1600	-.00922	-.00922	-.00922	.02376	299	.01001	7474	2278	1.562
6-A-6-2							361	.01001	9030	2752	1.562
6-A-6-3							357	.01002	8899	2712	1.636

[a]Model designations of references 4 and 5.

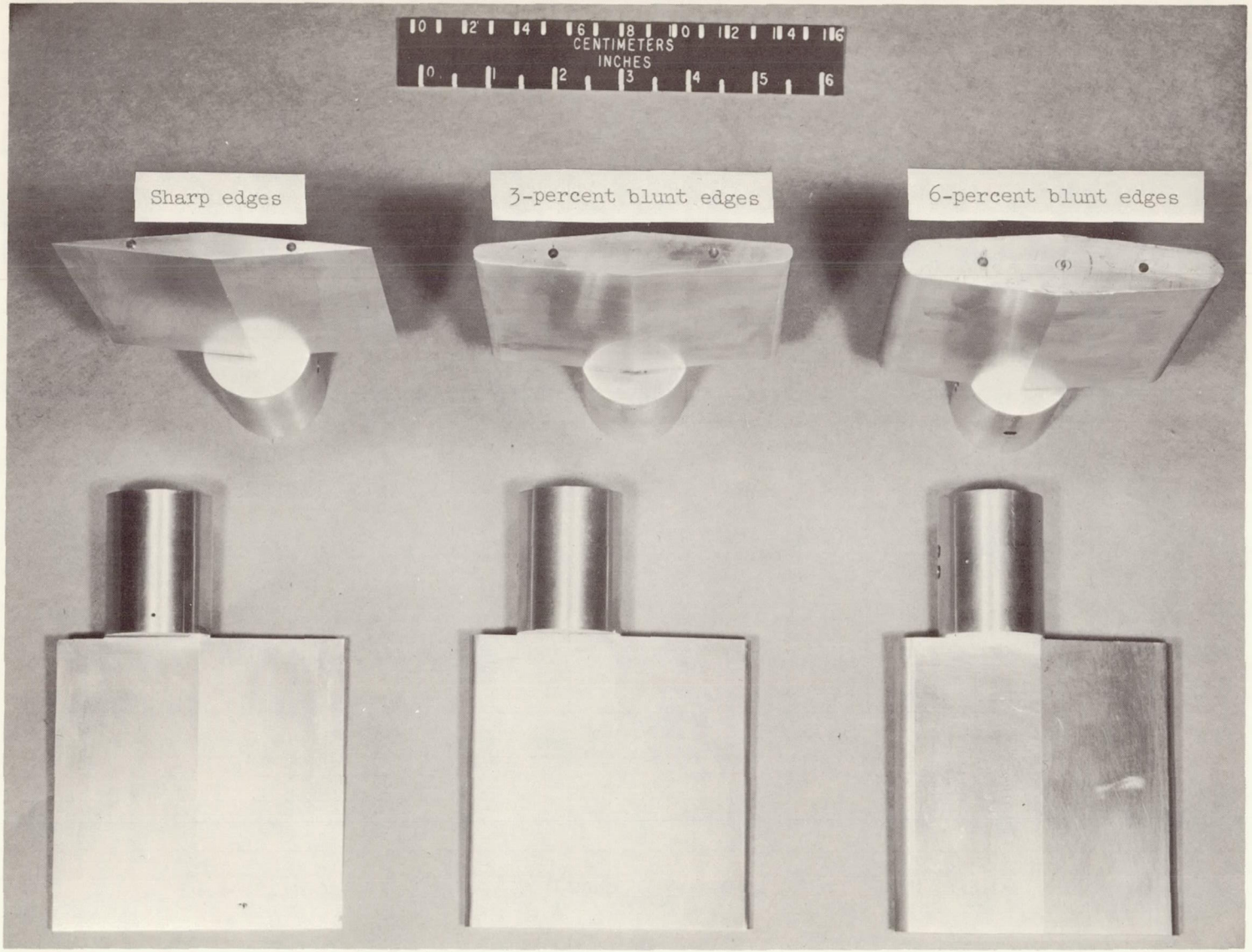

Figure 1.- Series of models for which static aerodynamic characteristics were determined at M = 6.8. c = 4 in. (10.16 cm). L-66-9046.1

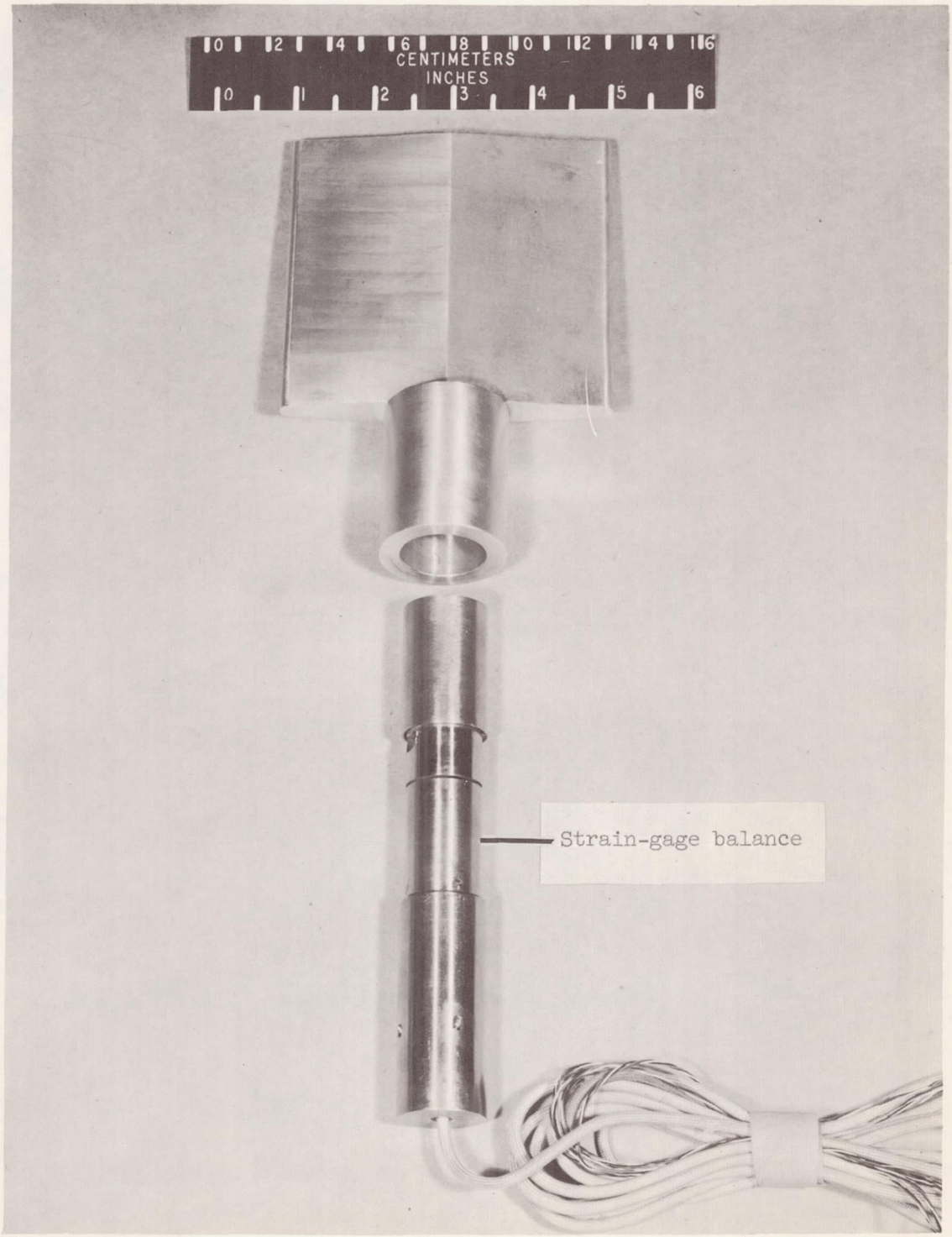

Figure 2.- Model and strain-gage balance assembly. L-66-9045.1

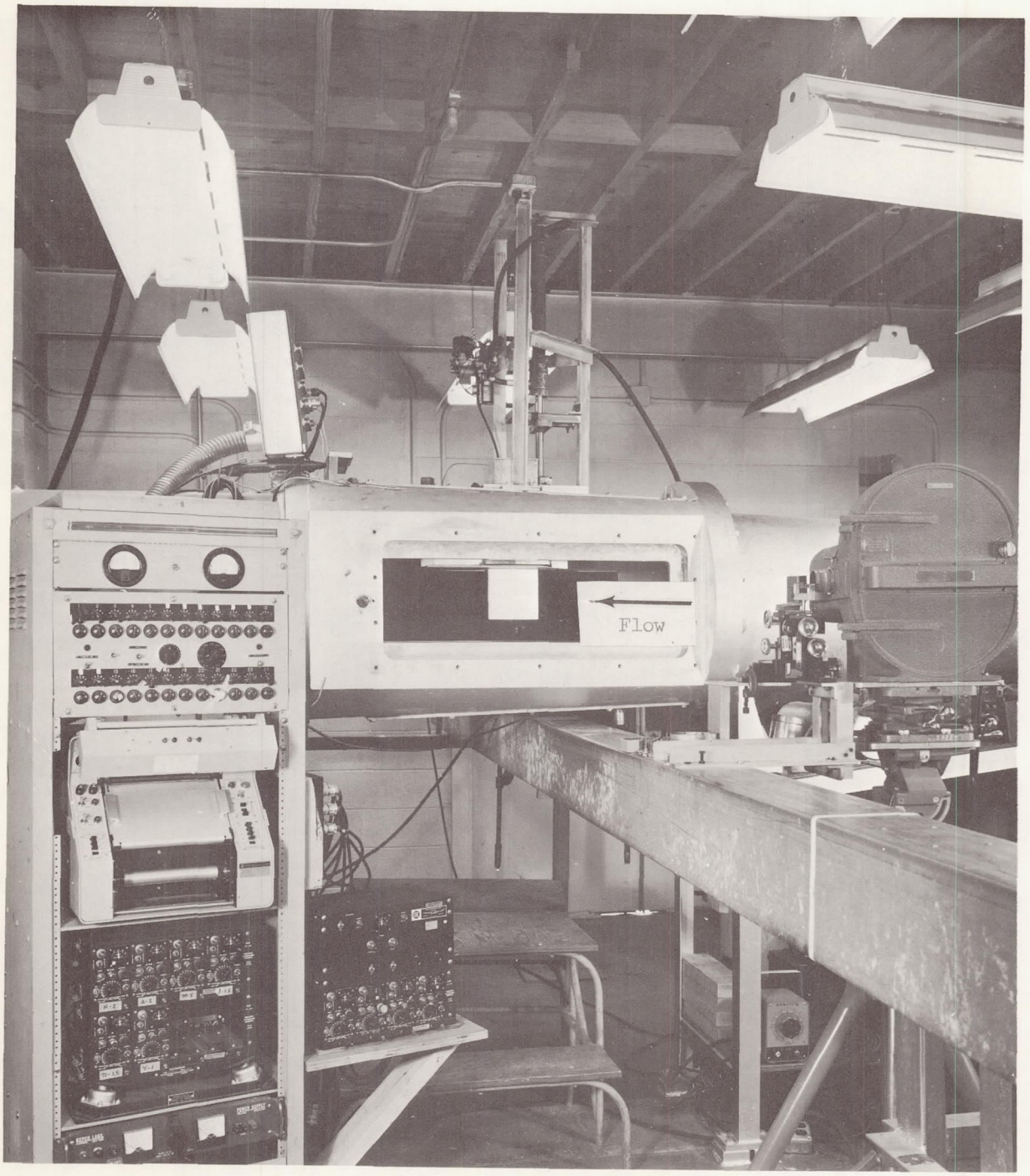

(a) Model position. L-66-5193.1

Figure 3.- Model with 6-in. (15.24-cm) chord mounted in the Mach 15 hypersonic aeroelasticity tunnel.

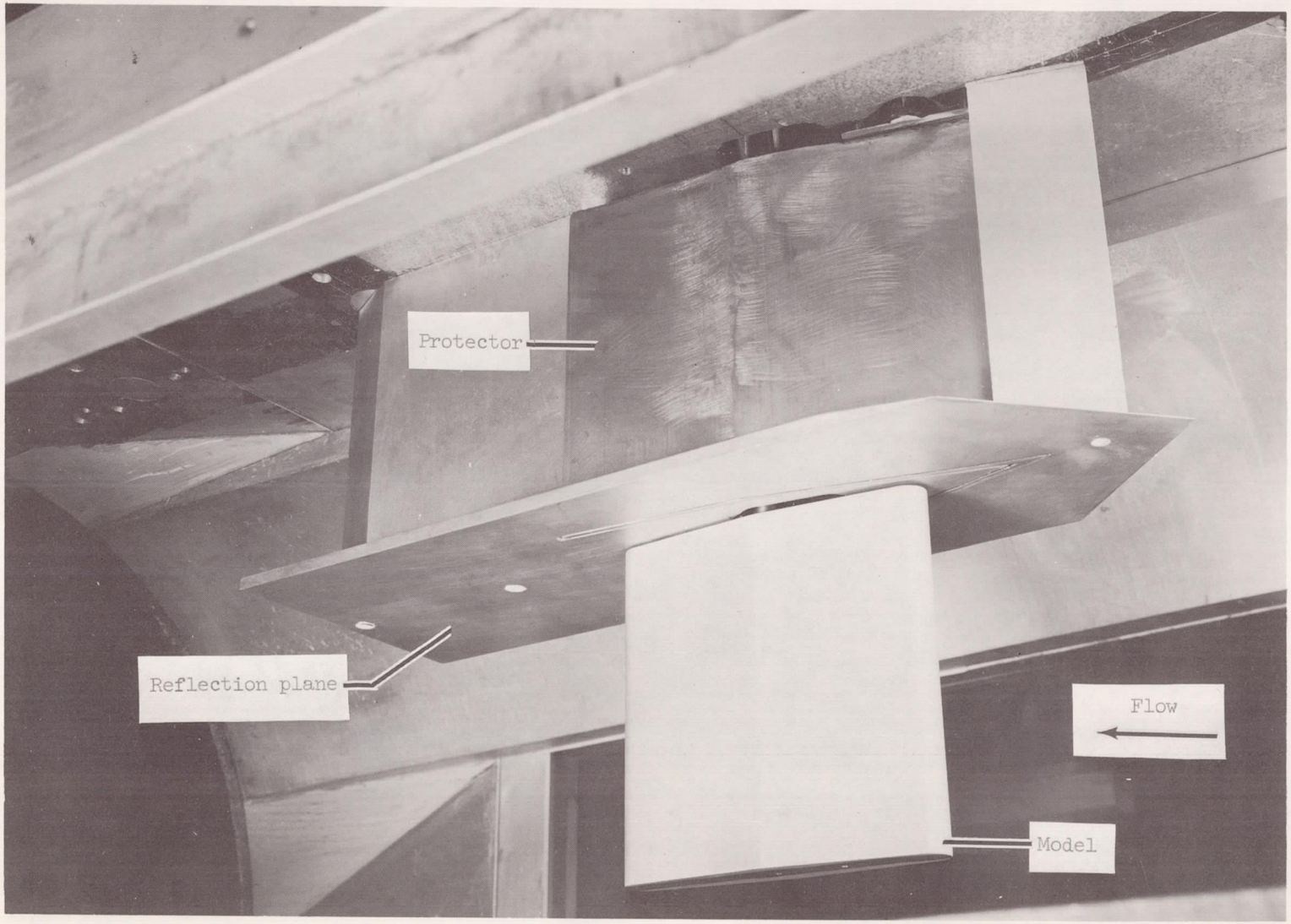

(b) Model support structure (protector retracted). L-66-5192

Figure 3.- Continued.

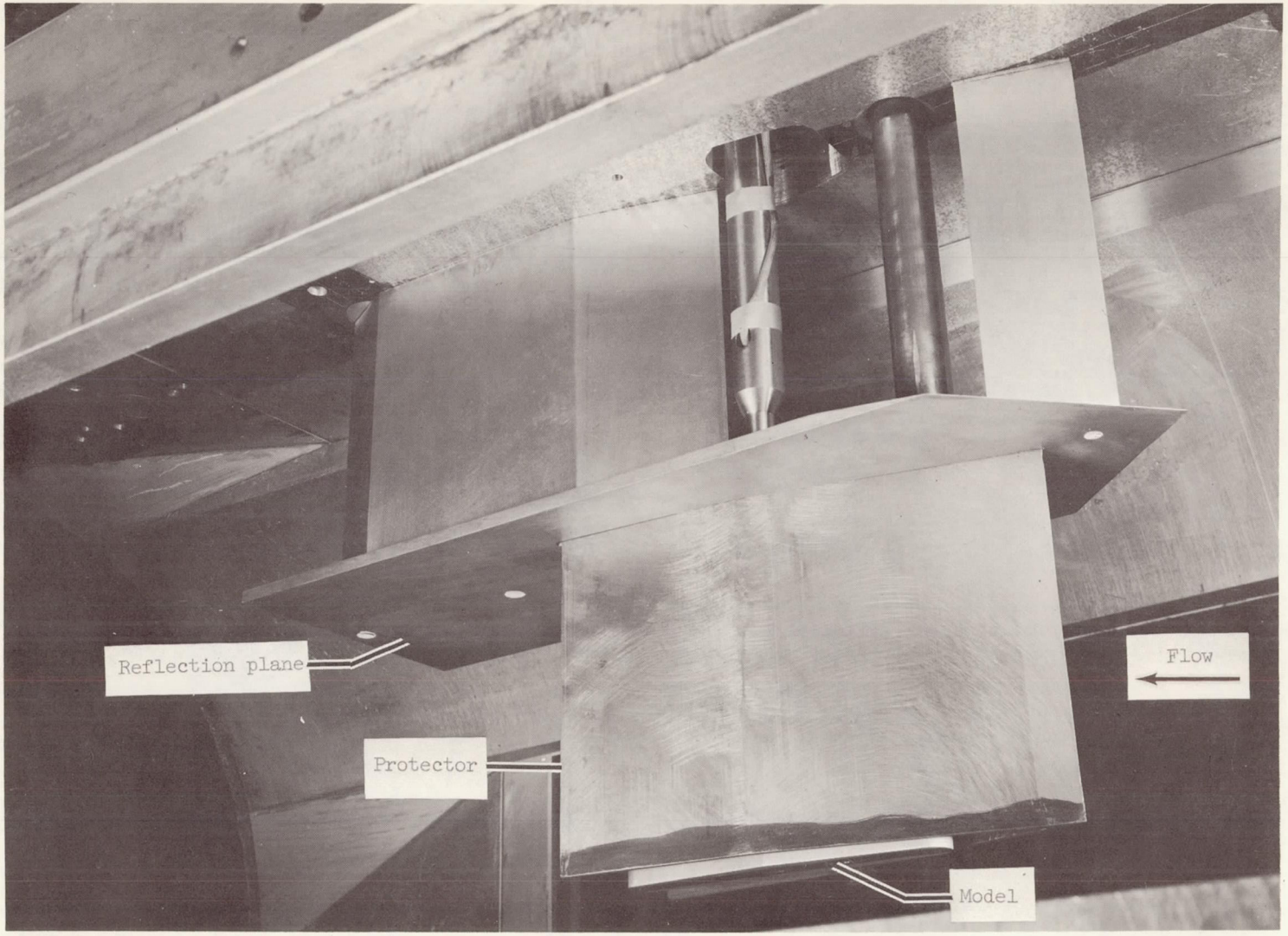

(c) Model protector extended.

L-66-5191.1

Figure 3.- Concluded.

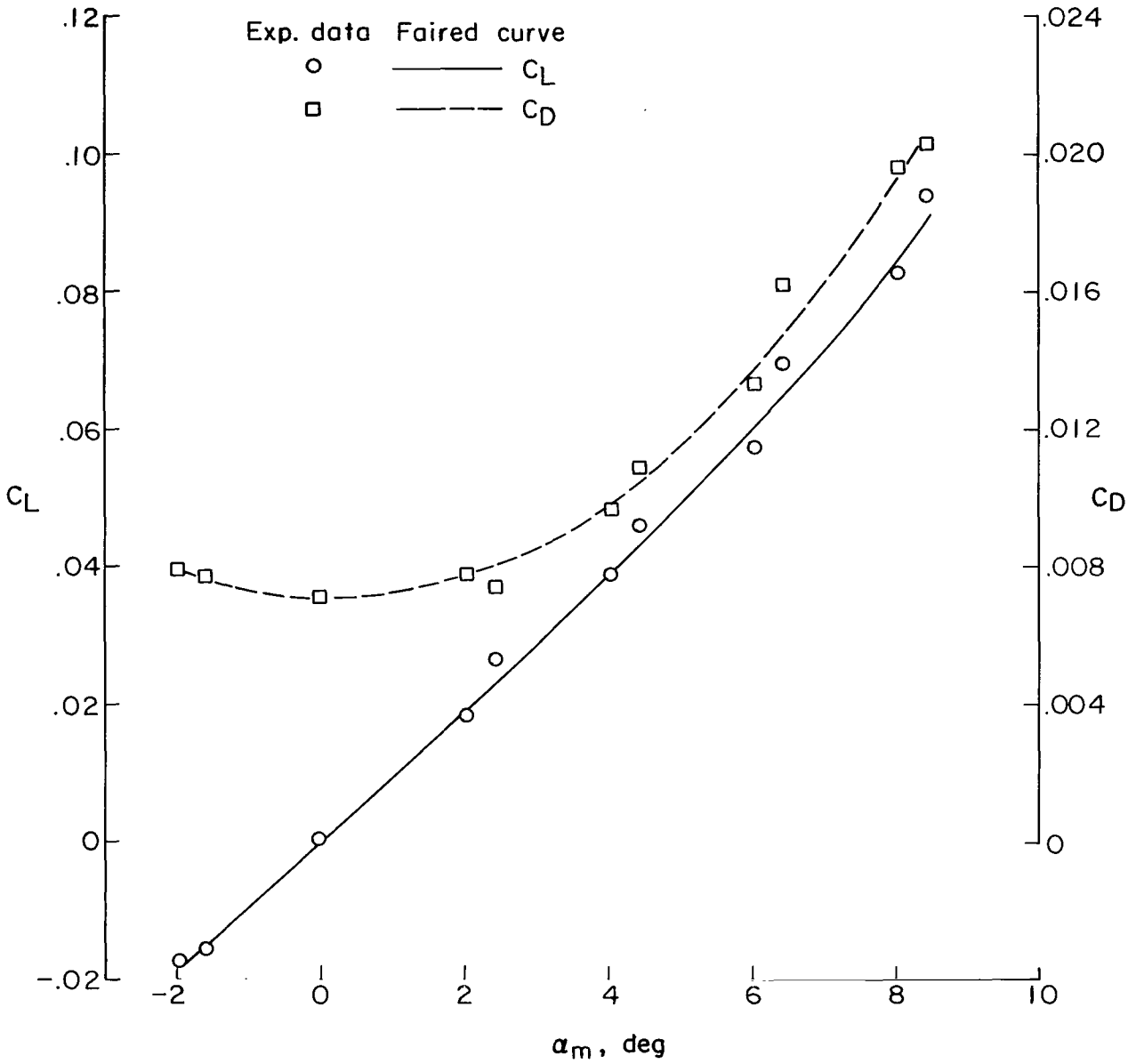

(a) Lift and drag.

Figure 4.- Characteristics of a sharp double-wedge airfoil at M = 6.8.

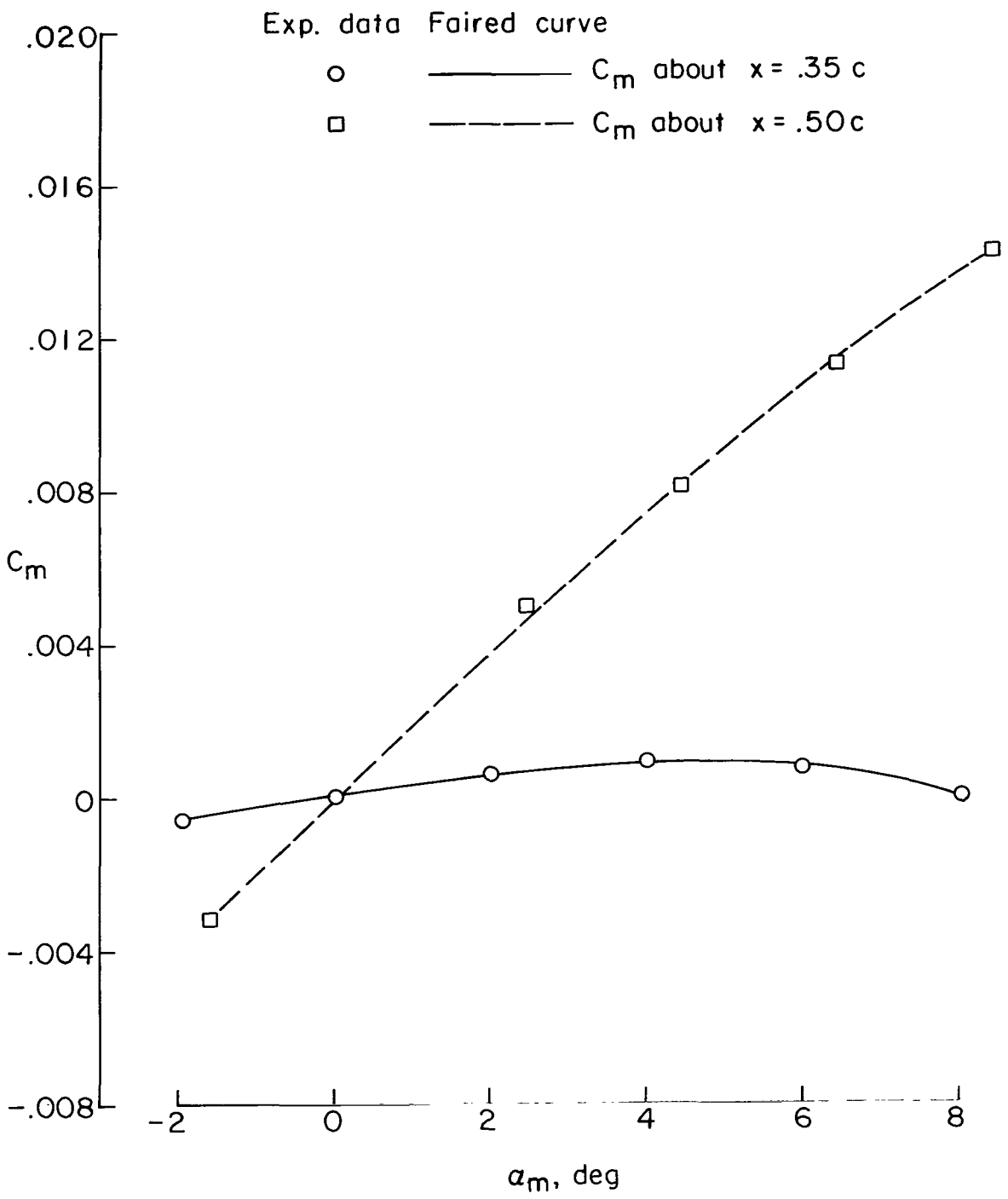

(b) Pitching moment.

Figure 4.- Concluded.

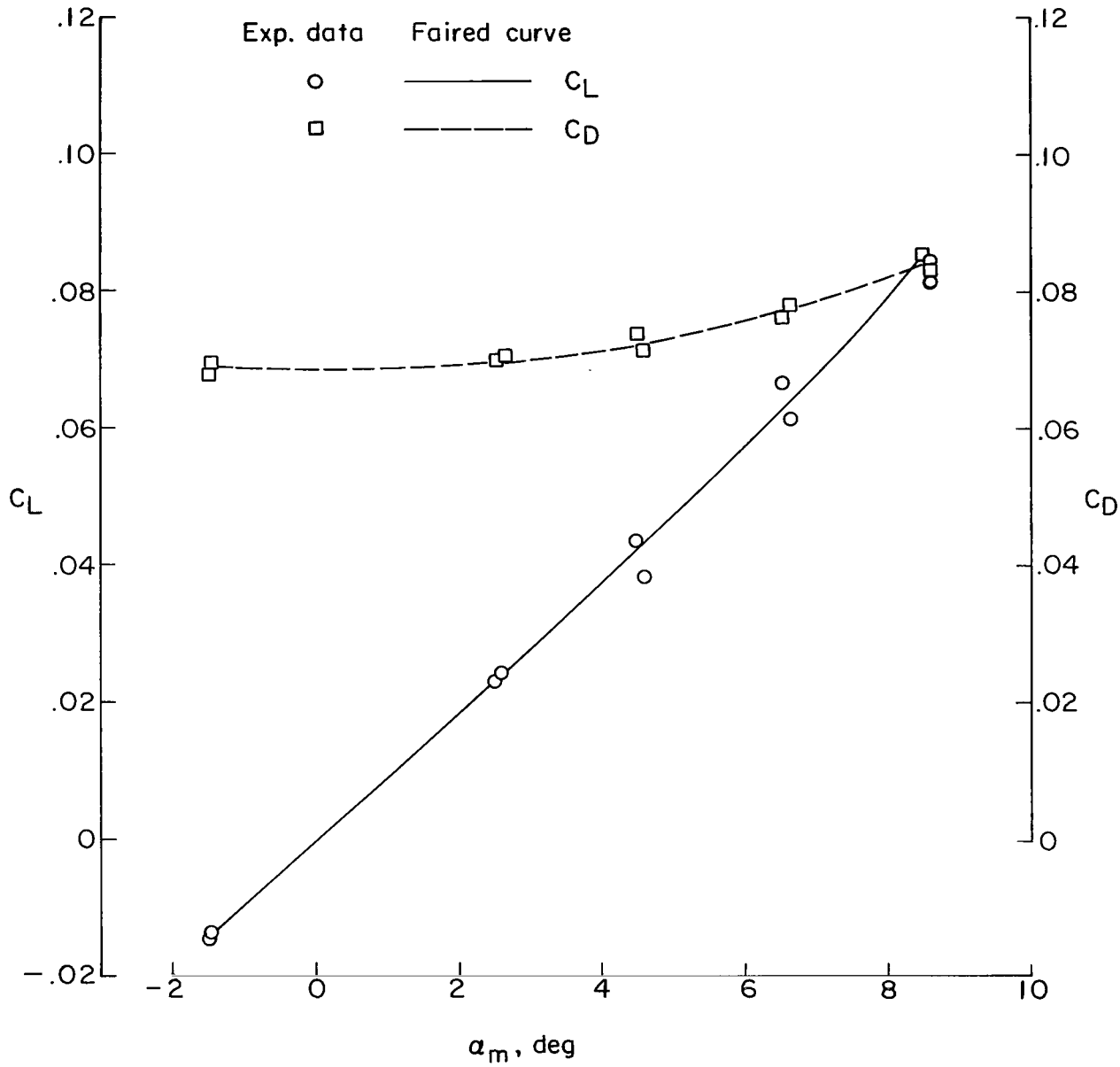

(a) Lift and drag.

Figure 5.- Characteristics of a 3-percent blunt double-wedge airfoil at M = 6.8.

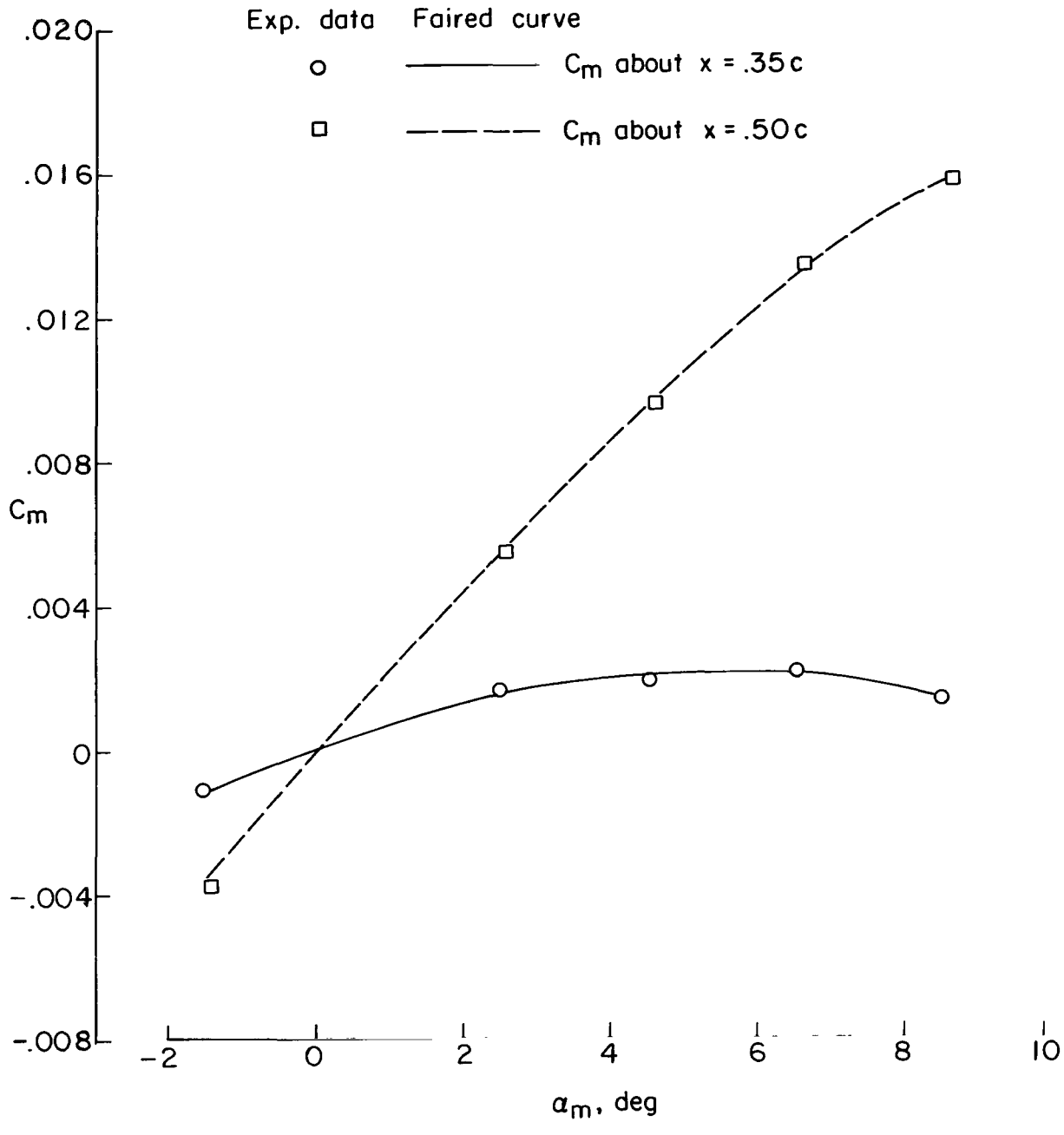

(b) Pitching moment.

Figure 5.- Concluded.

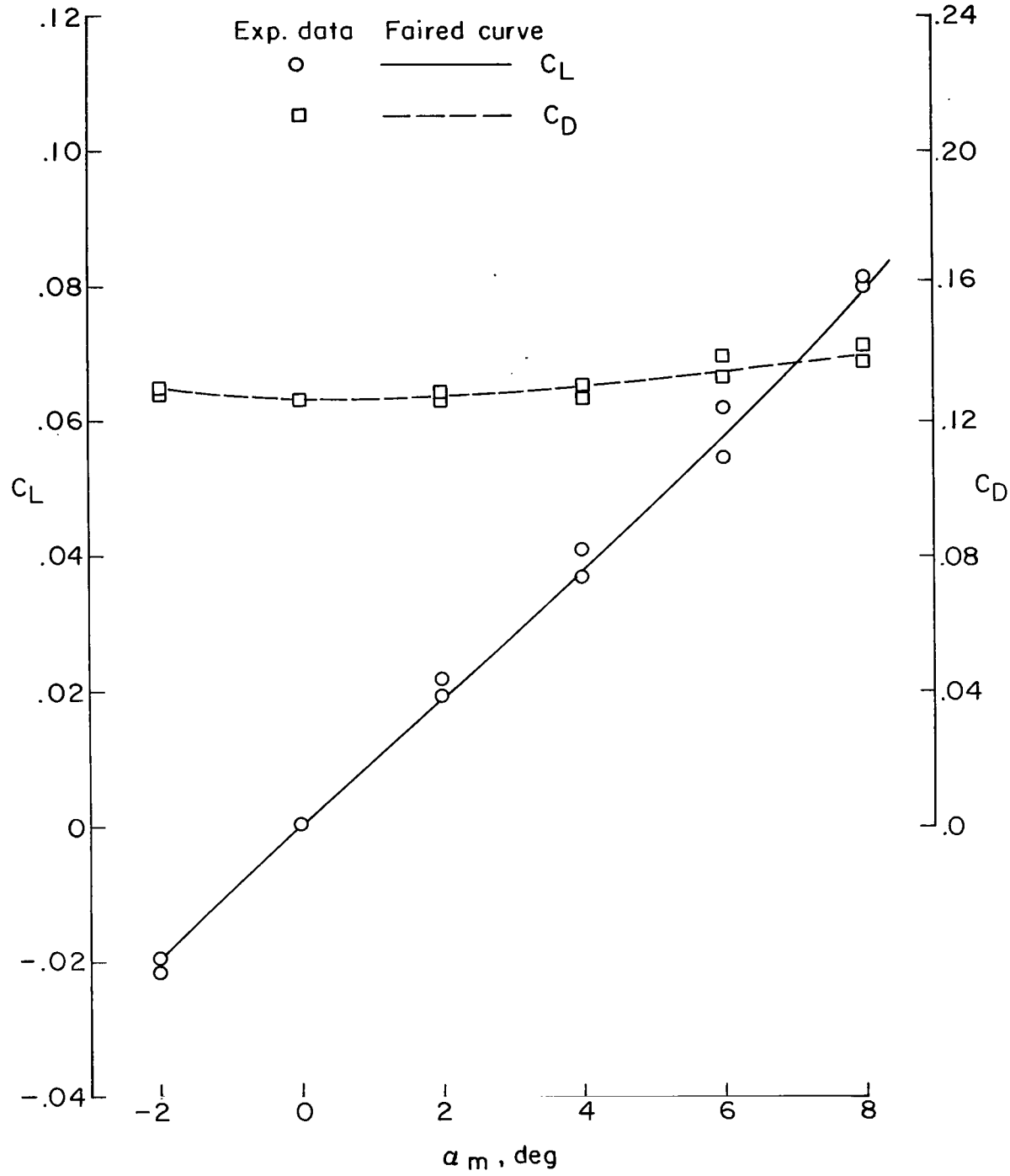

(a) Lift and drag.

Figure 6.- Characteristics of a 6-percent blunt double-wedge airfoil at M = 6.8.

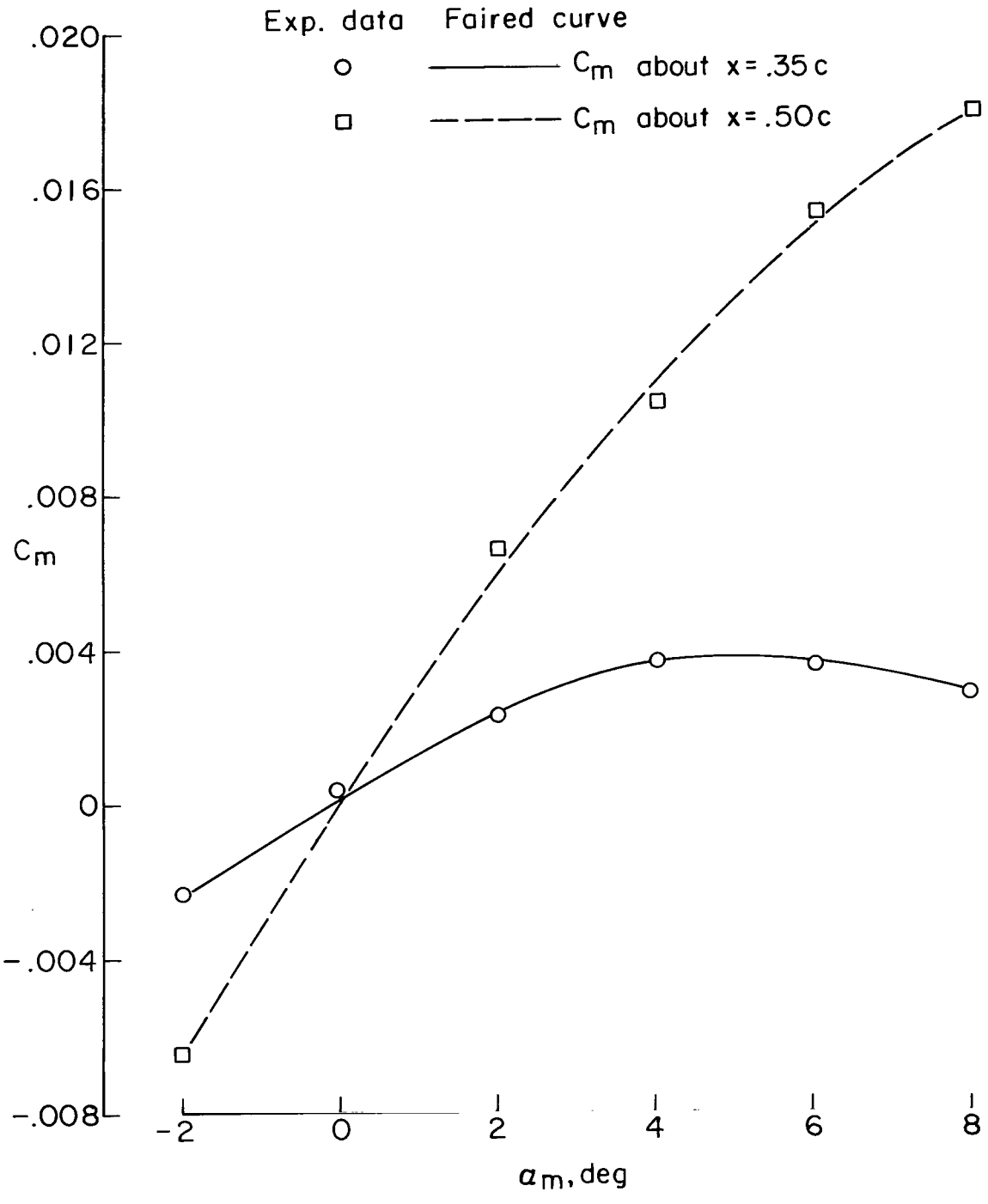

(b) Pitching moment.

Figure 6.- Concluded.

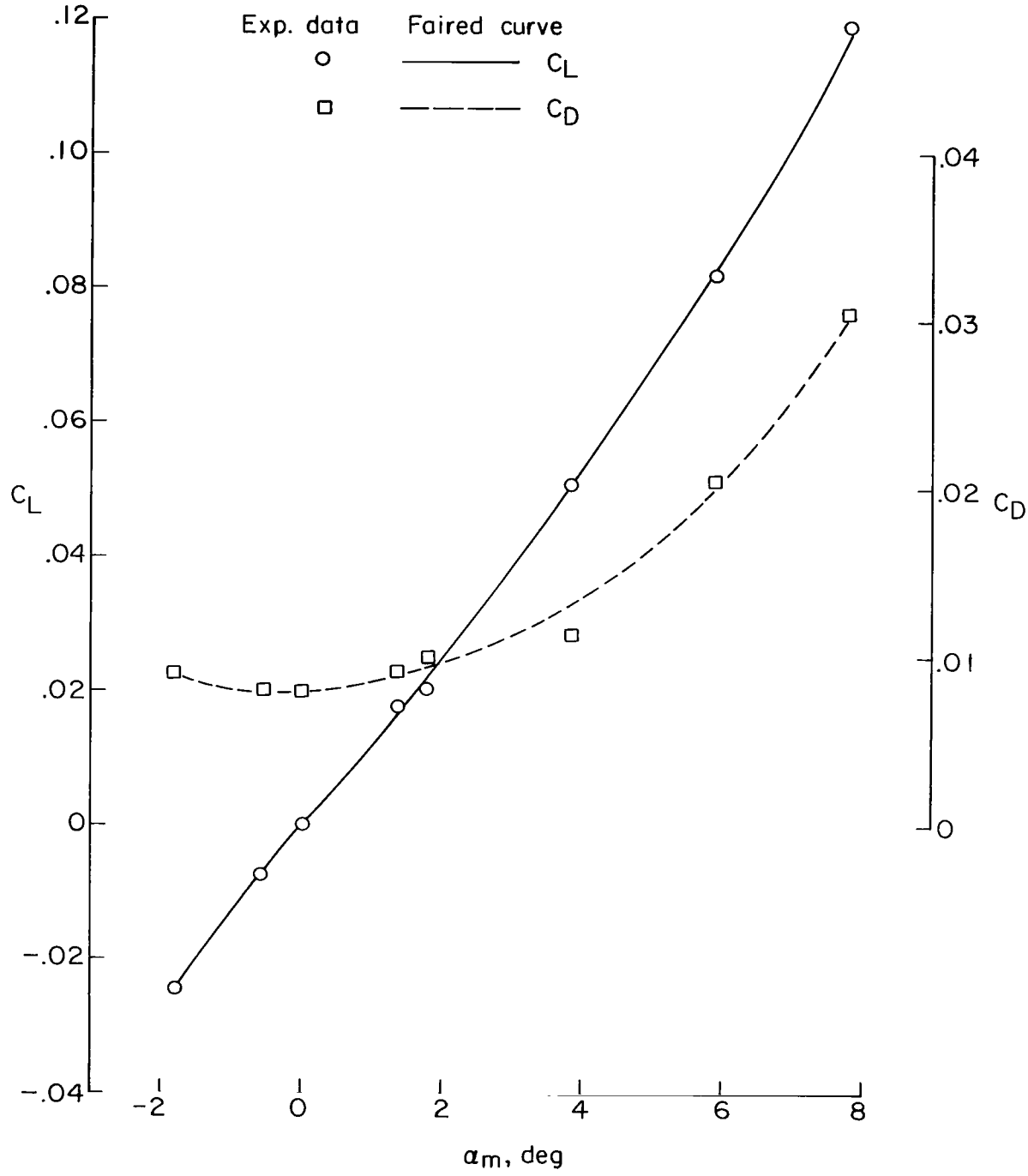

(a) Lift and drag.

Figure 7.- Characteristics of a sharp double-wedge airfoil at M = 15.3.

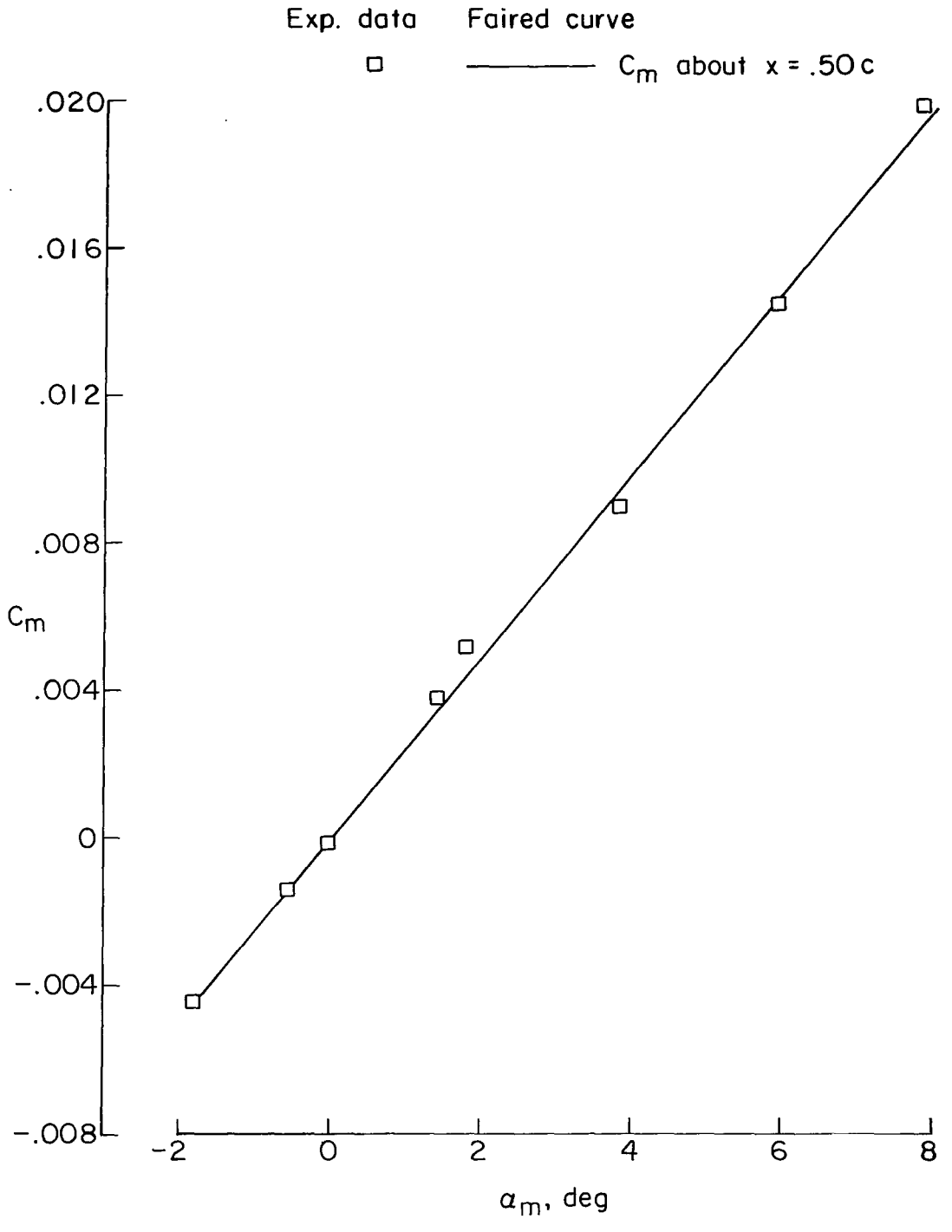

(b) Pitching moment.

Figure 7.- Concluded.

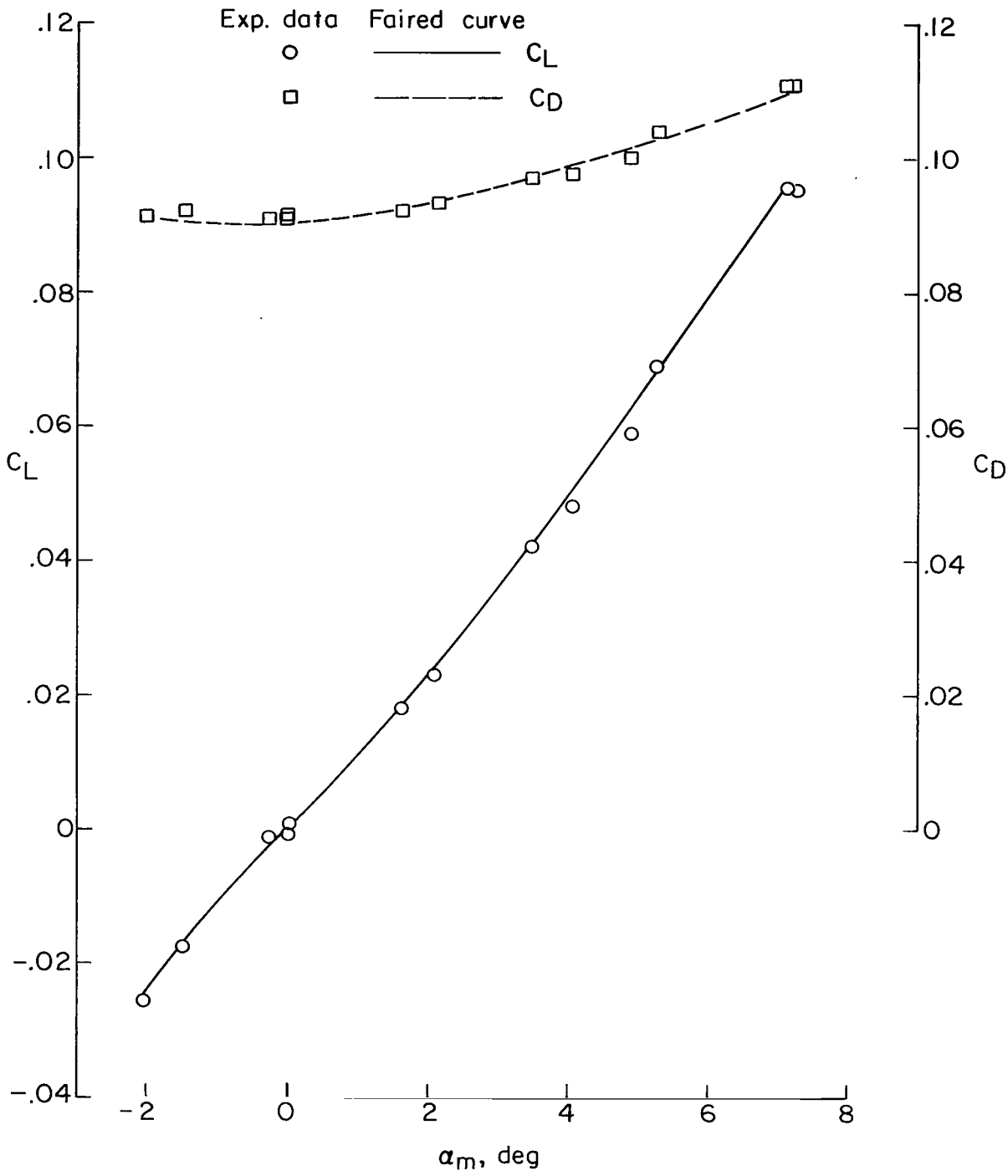

(a) Lift and drag.

Figure 8.- Characteristics of a 3-percent blunt double-wedge airfoil at M = 15.3.

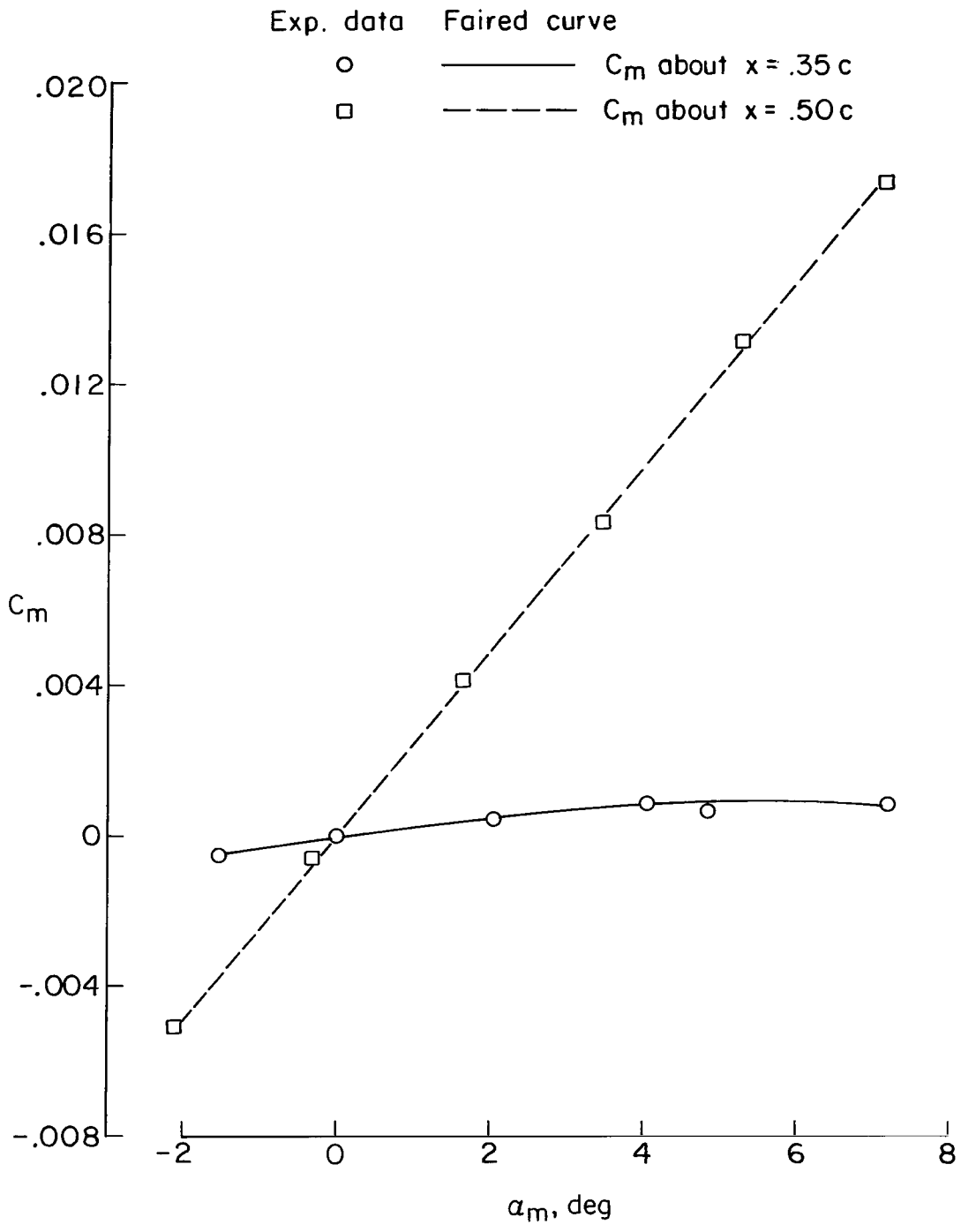

(b) Pitching moment.

Figure 8.- Concluded.

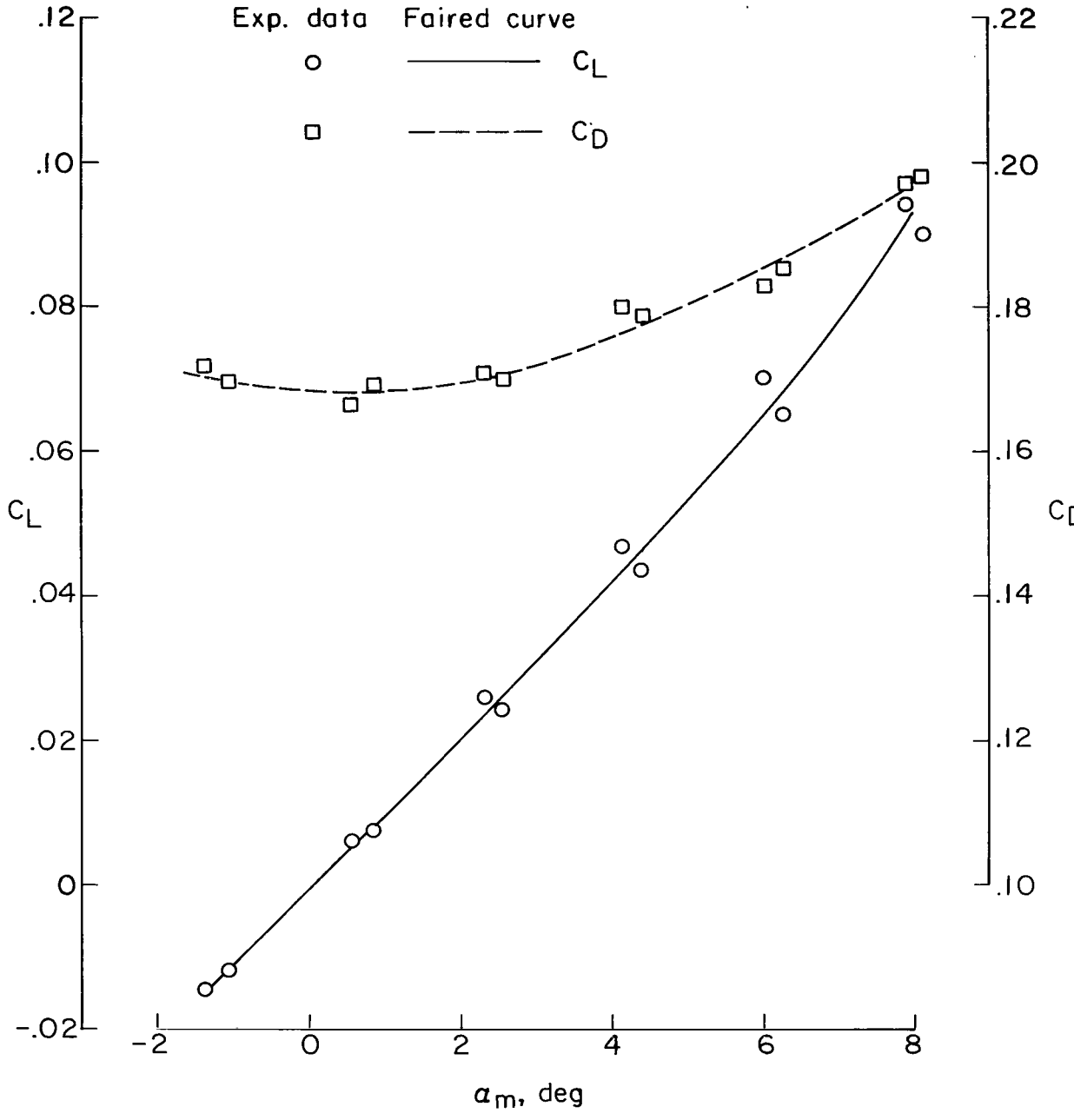

(a) Lift and drag.

Figure 9.- Characteristics of a 6-percent blunt double-wedge airfoil at M = 15.3.

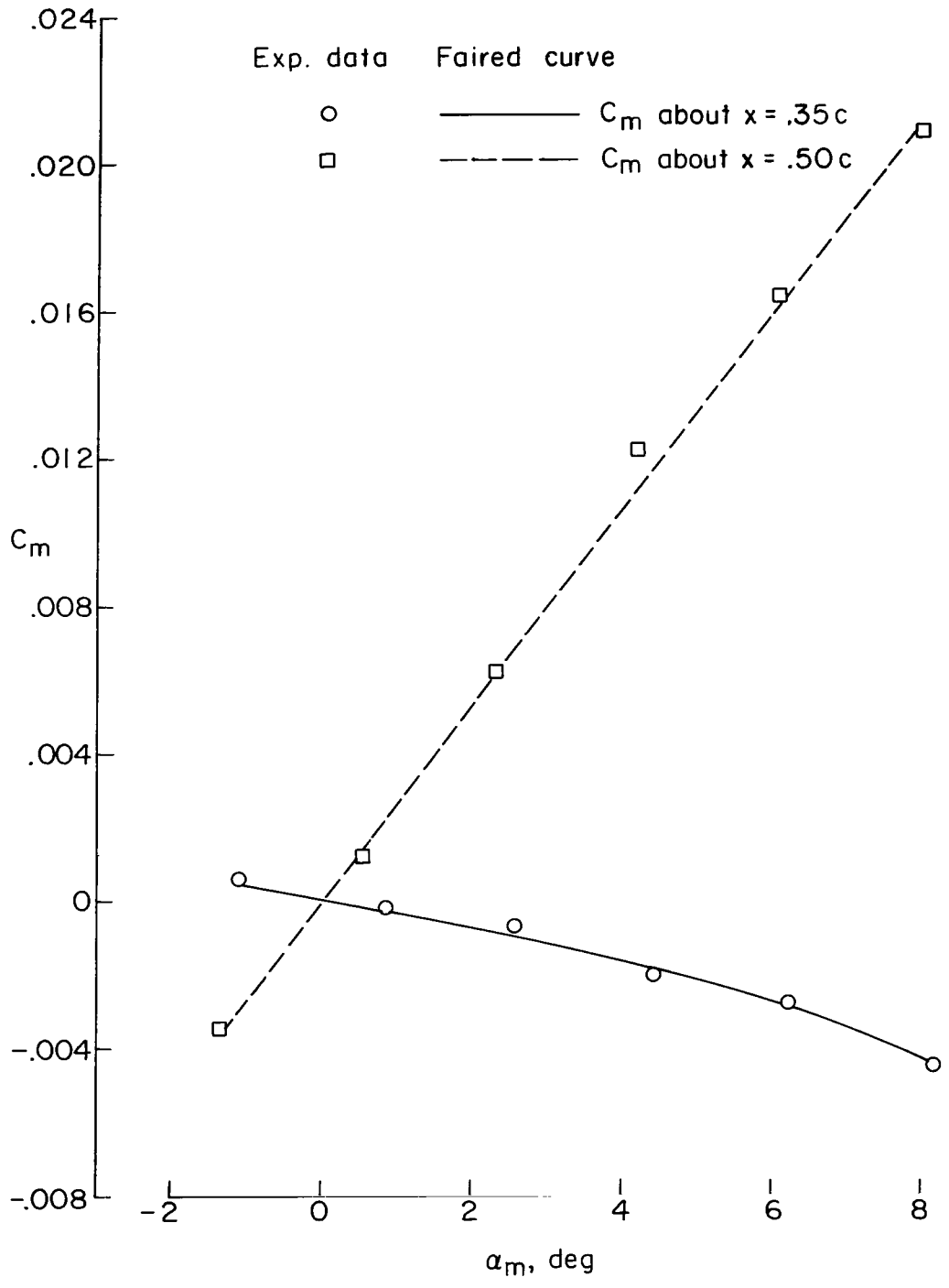

(b) Pitching moment.

Figure 9.- Concluded.

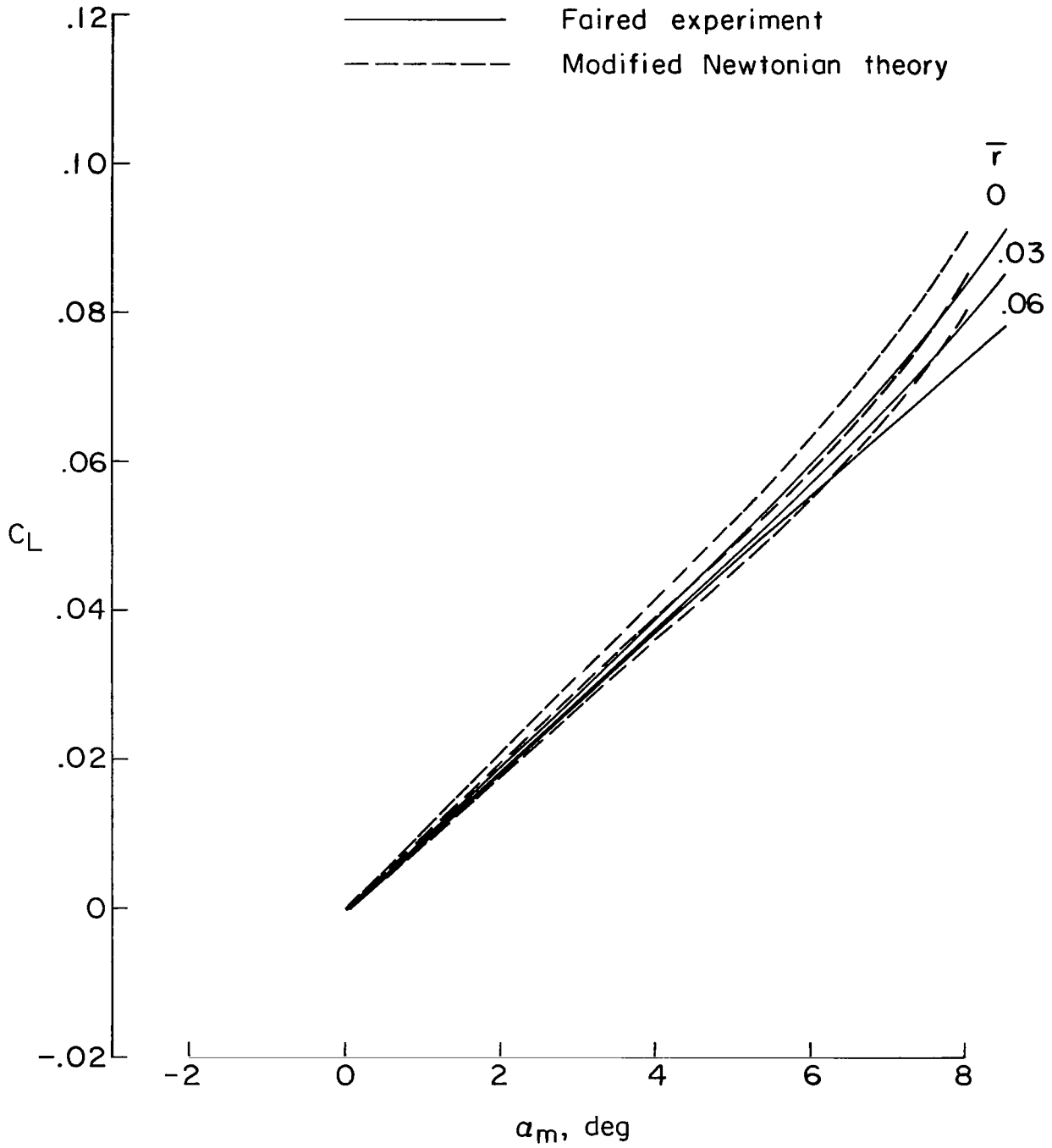

(a) M = 6.8.

Figure 10.- Effect of leading-edge bluntness on the lift characteristics of a 5^0 double-wedge airfoil.

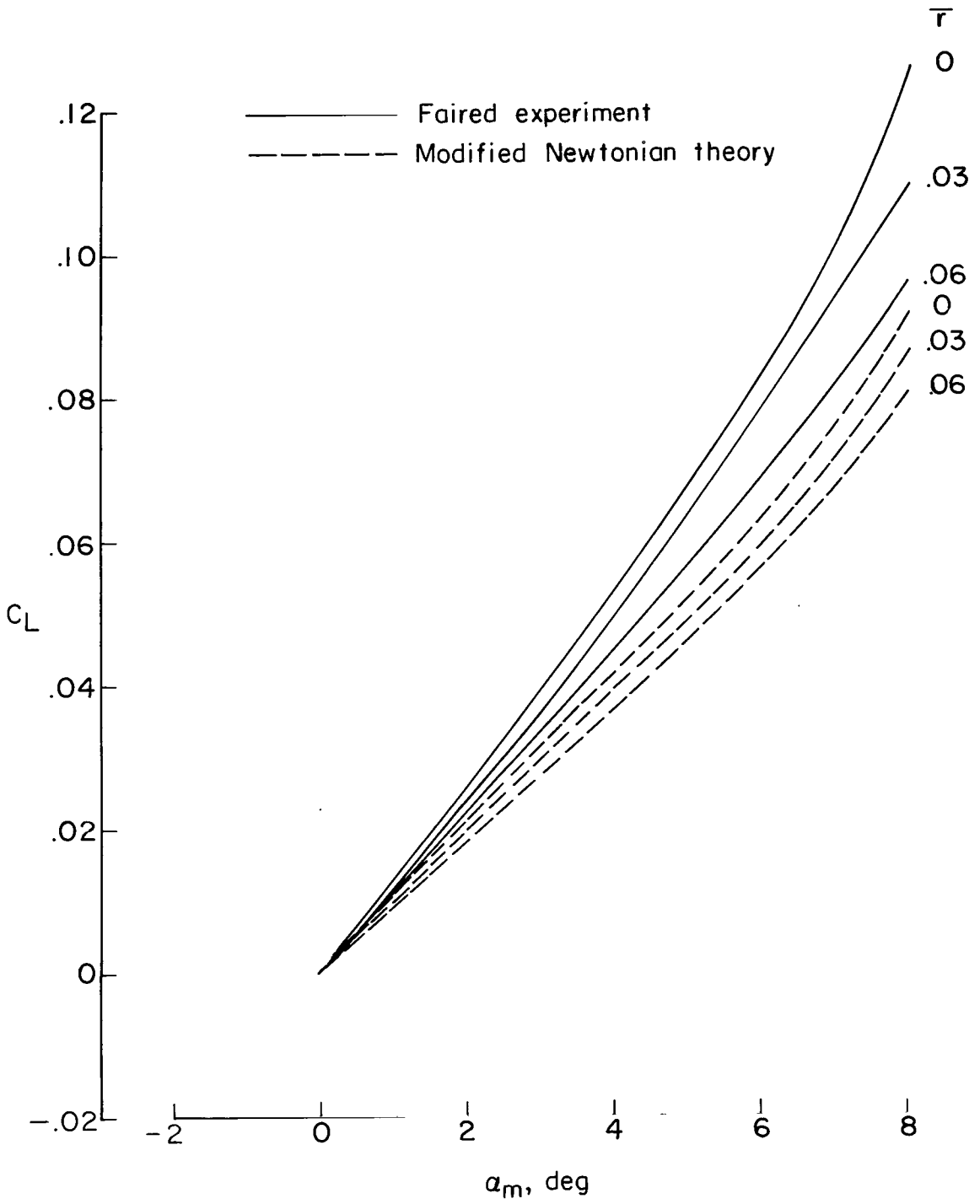

(b) M = 15.3.

Figure 10.- Concluded.

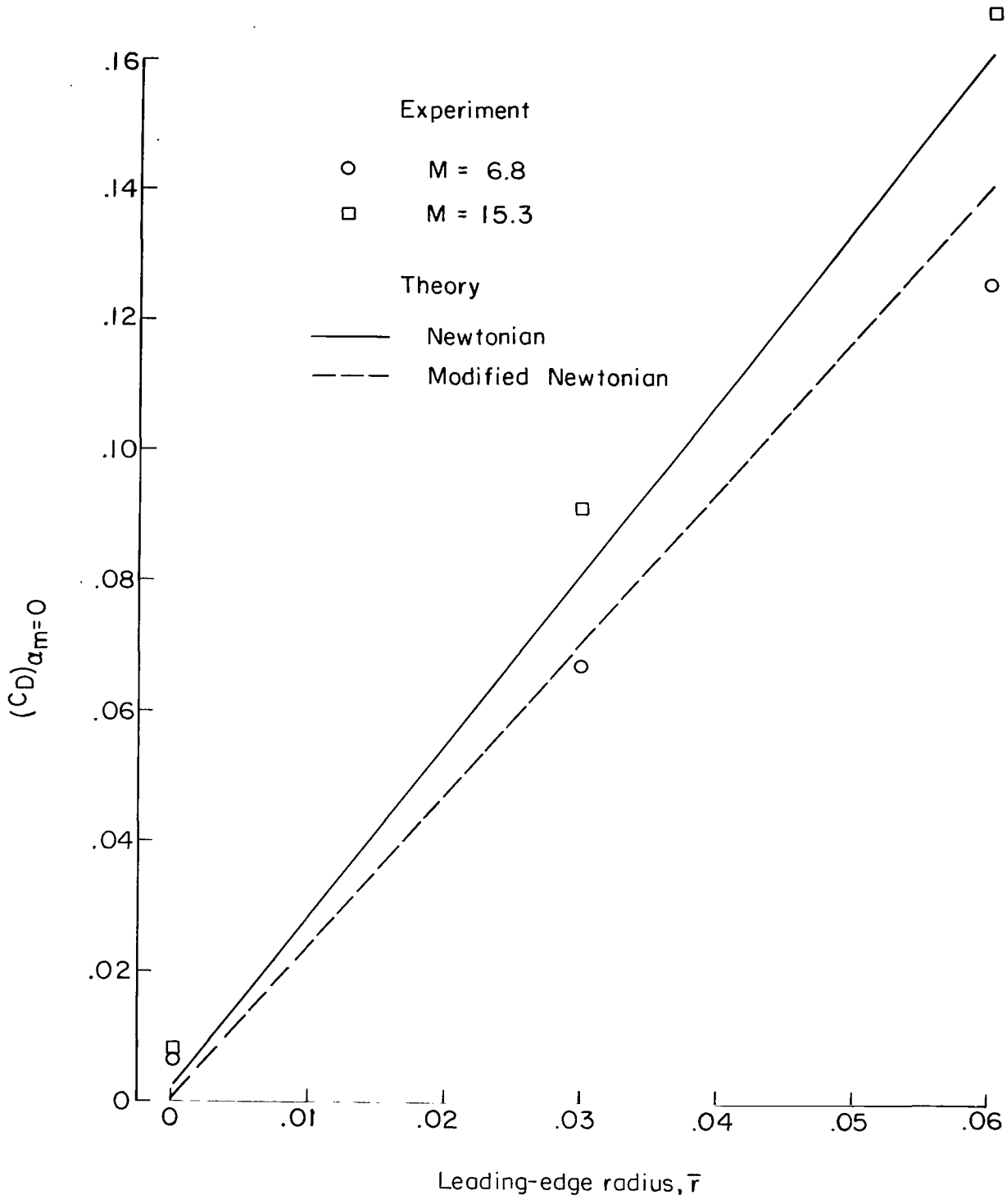

Figure 11.- Effect of leading-edge bluntness on the drag characteristics of a 5° double-wedge airfoil at $\alpha_m = 0°$.

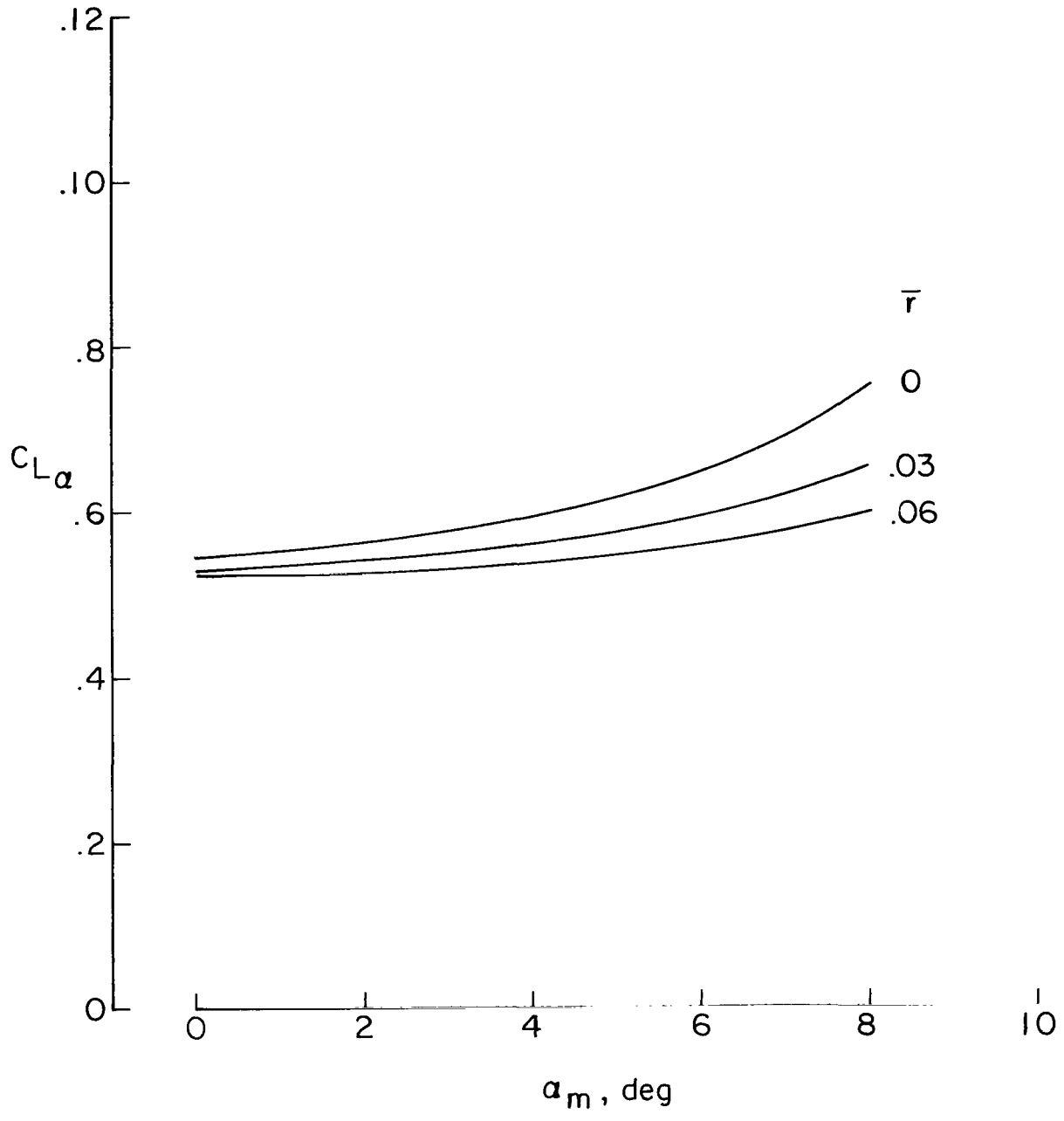

(a) M = 6.8.

Figure 12.- Lift-curve slopes for the series of double-wedge airfoils (from faired experimental curves).

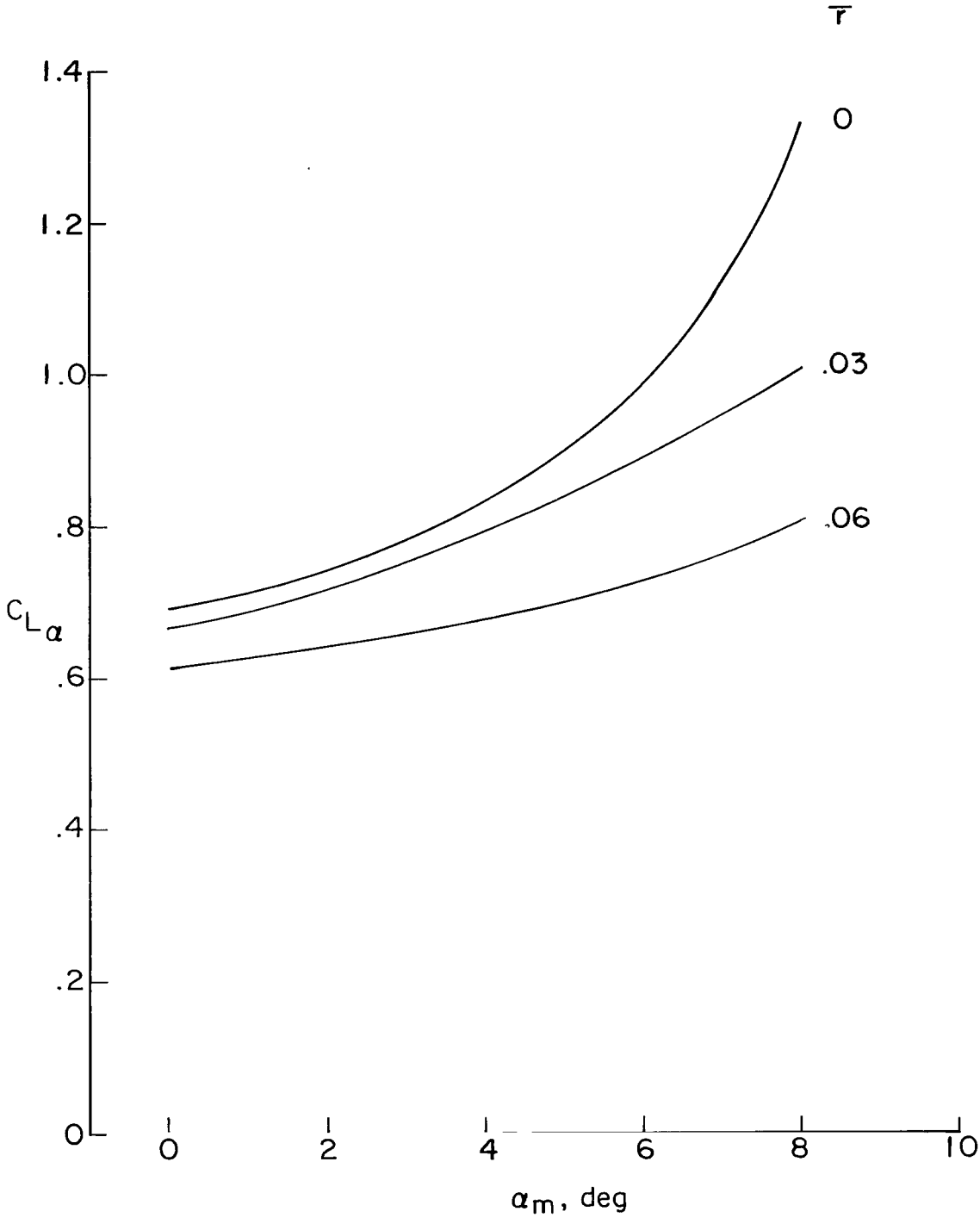

(b) M = 15.3.

Figure 12.- Concluded.

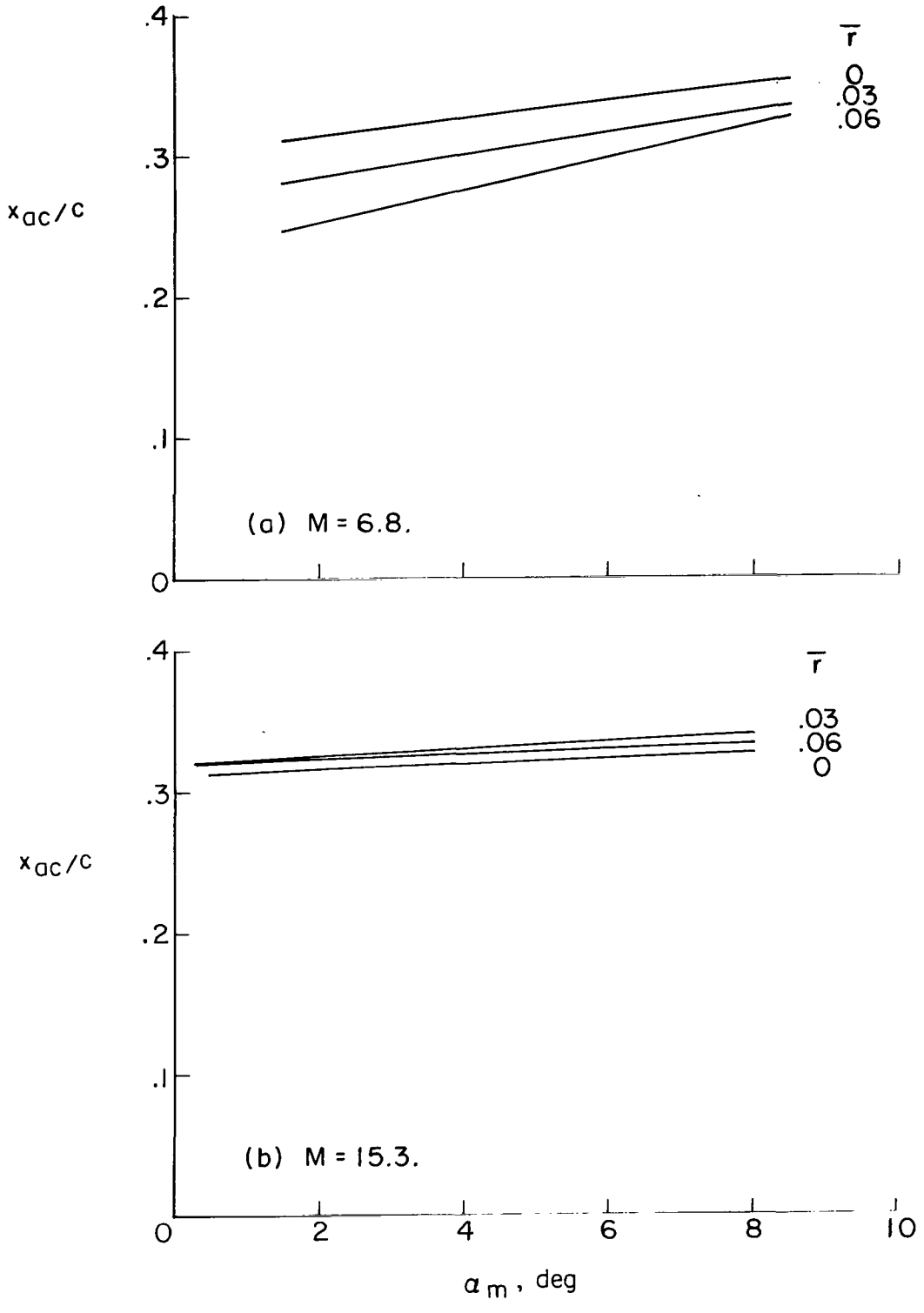

Figure 13.- Aerodynamic-center locations for the series of double-wedge airfoils (from faired experimental curves).

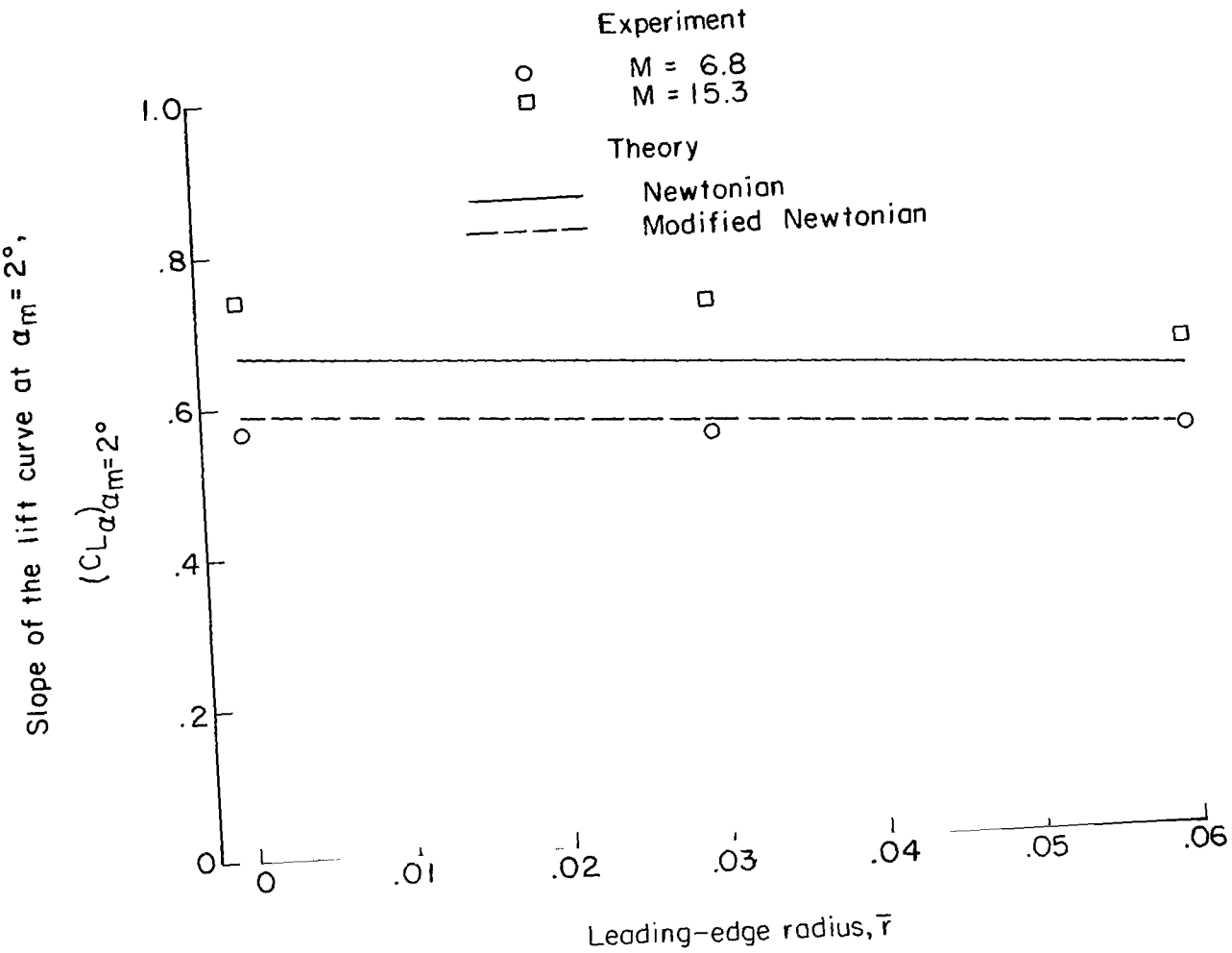

Figure 14.- Effect of leading-edge bluntness on the slope of the lift curve for a 5° double-wedge airfoil at $\alpha_m = 2°$.

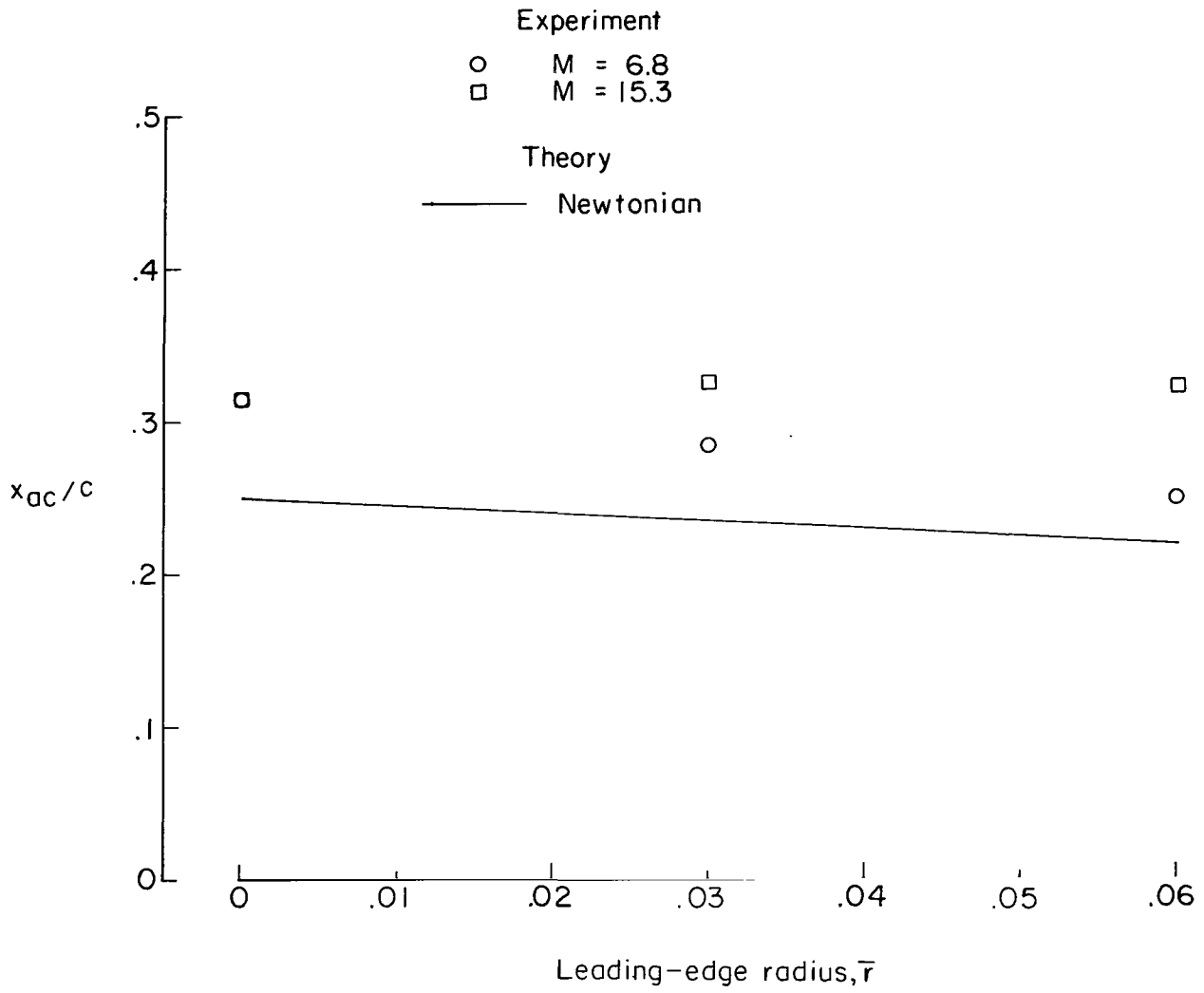

Figure 15.- Effect of leading-edge bluntness on the location of the aerodynamic center for a 5^0 double-wedge airfoil at $\alpha_m = 2^0$.

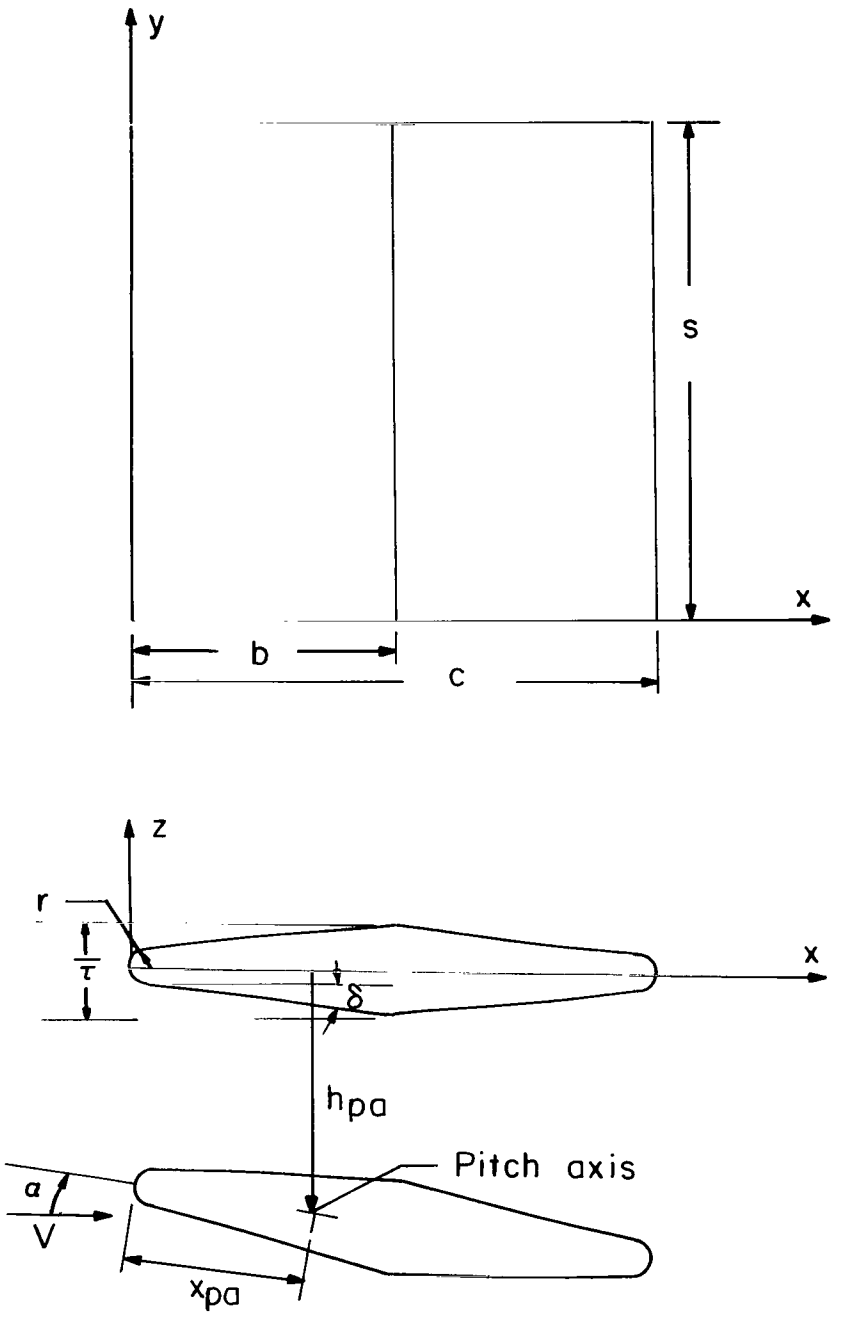

Figure 16.- Model configuration.

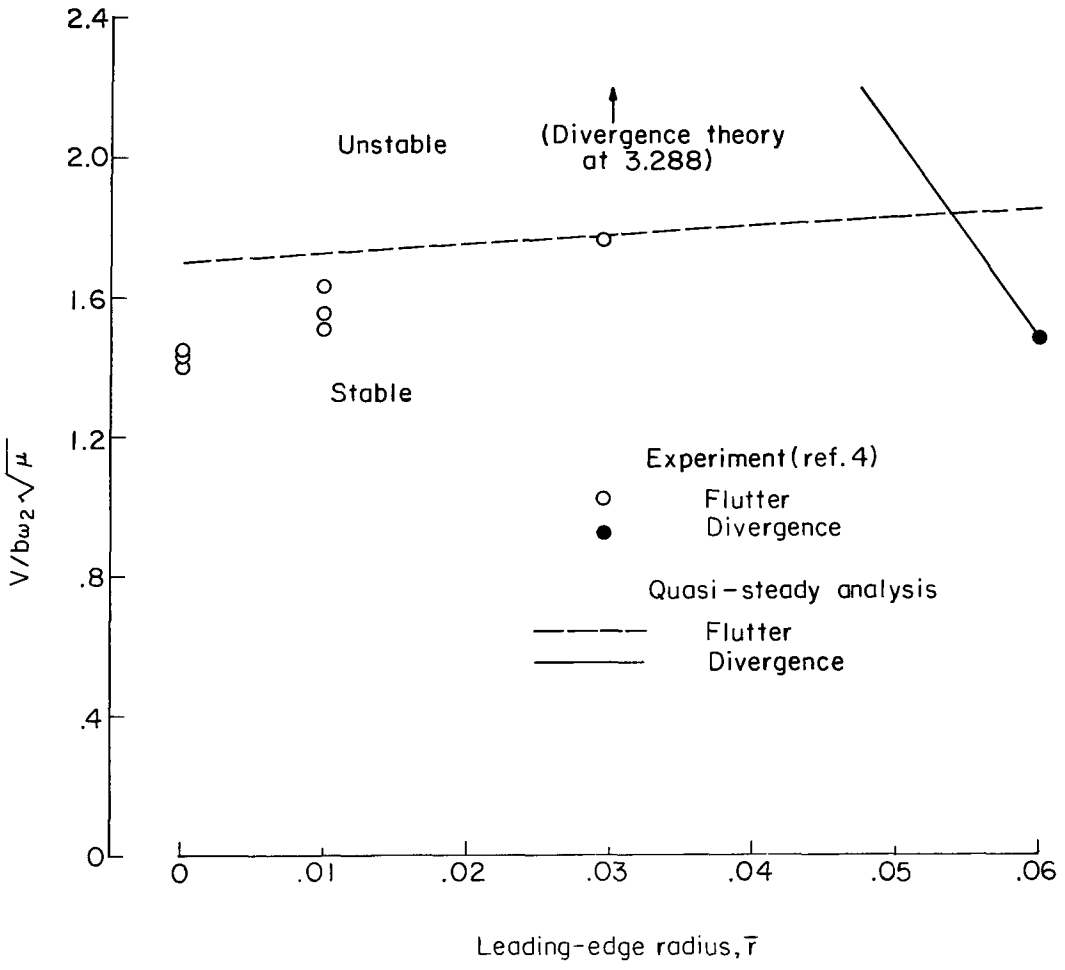

(a) M = 6.8.

Figure 17.- Velocity-index parameter as a function of leading-edge radius for a 5^0 double-wedge airfoil at $\alpha_m = 0^0$.

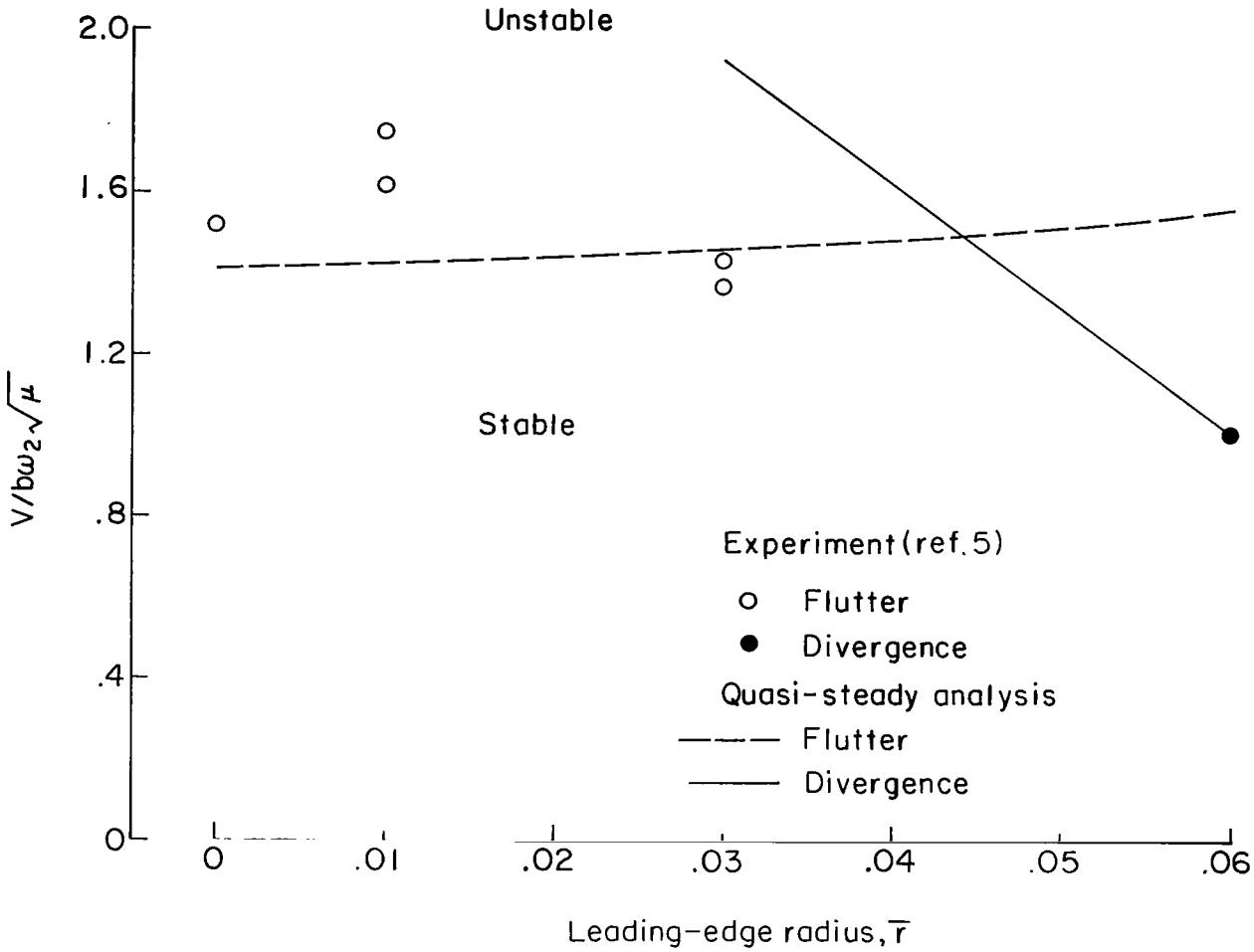

(b) M = 15.3.

Figure 17.- Concluded.

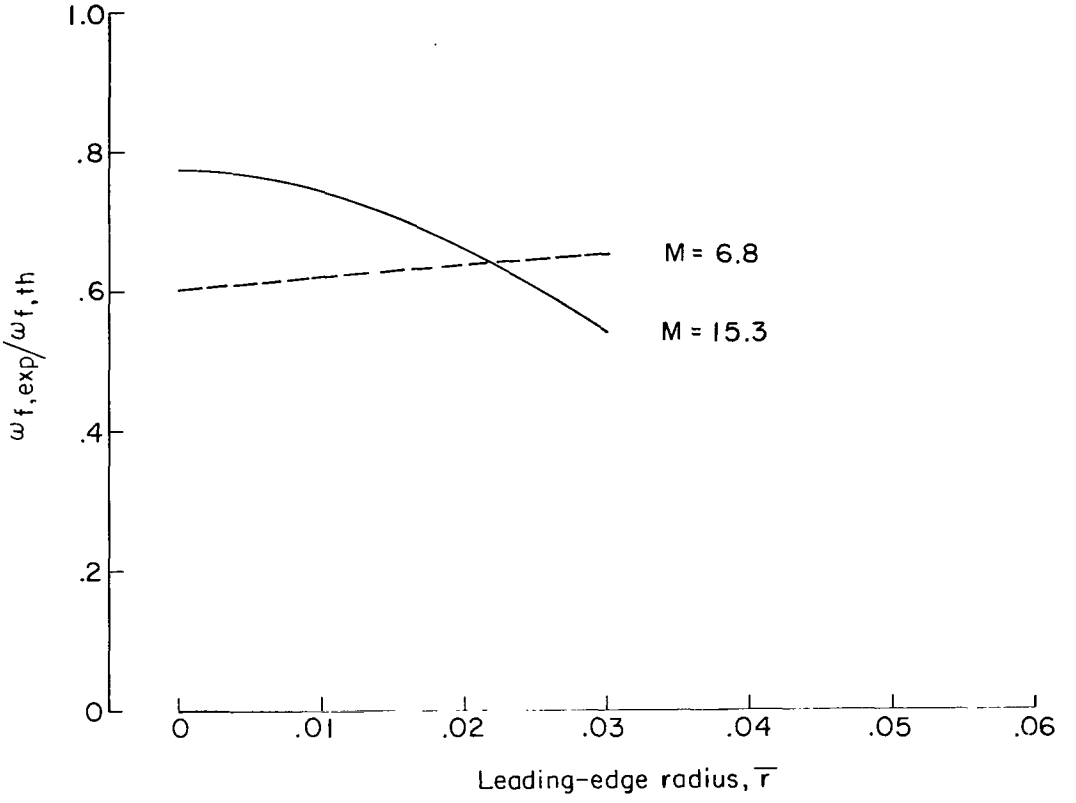

Figure 18.- Comparison of the experimental and quasi-steady flutter frequencies. $\alpha_m = 0^0$.

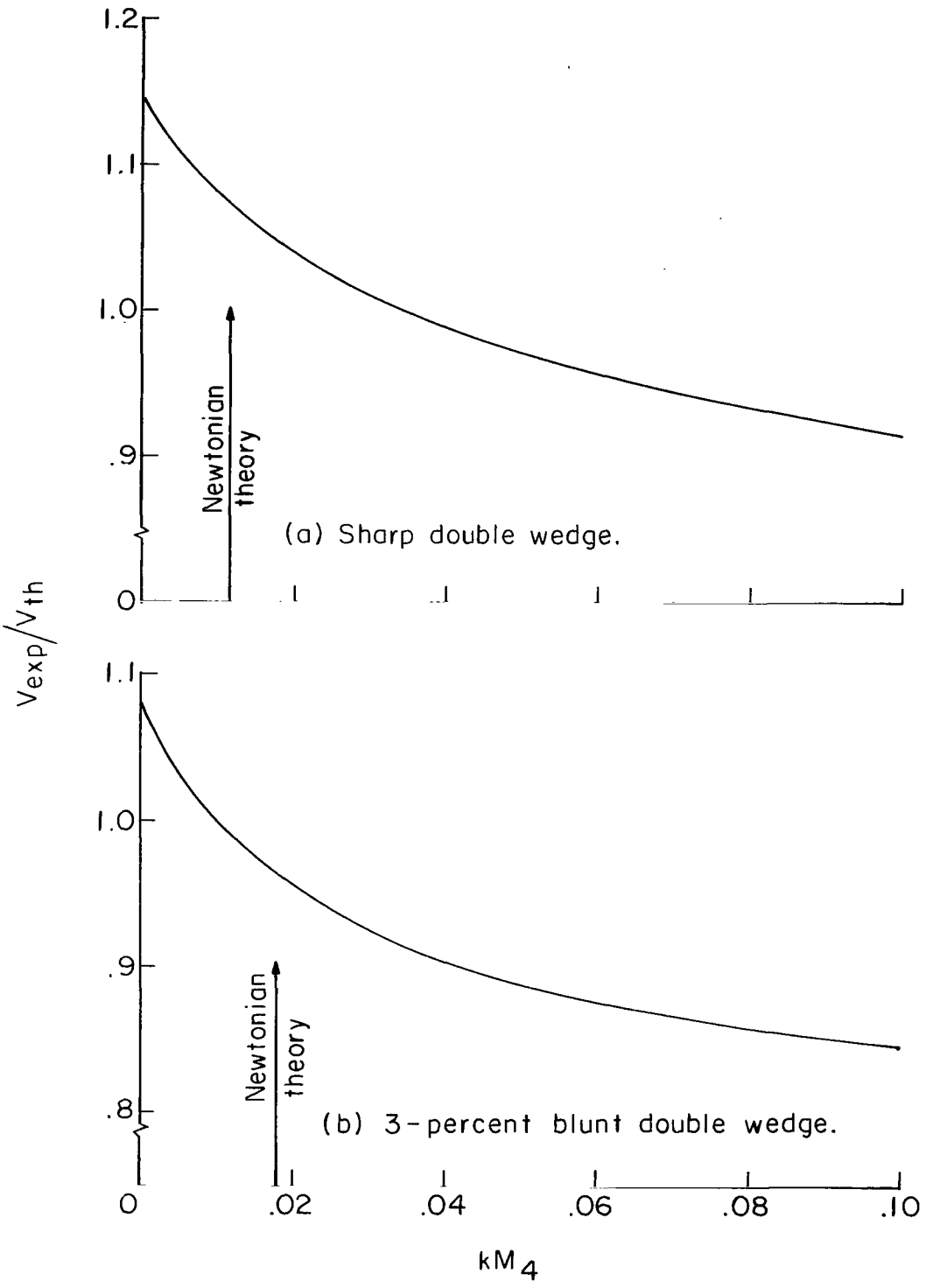

Figure 19.- Effect of M_4 on the quasi-steady flutter velocity at $M = 15.3$. $\alpha_m = 0^0$.

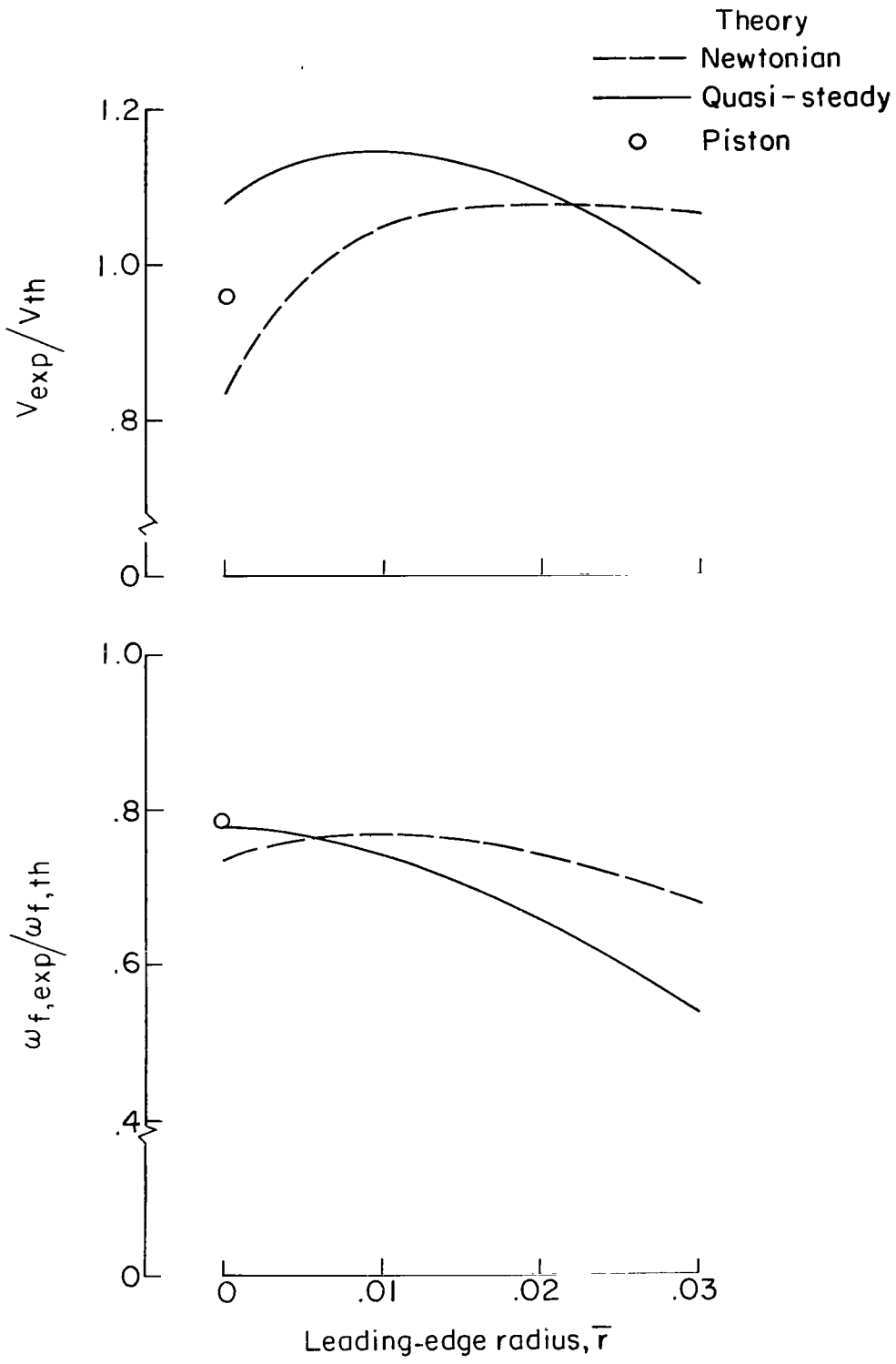

Figure 20.- Quasi-steady results compared with Newtonian and piston theory results at M = 15.3.

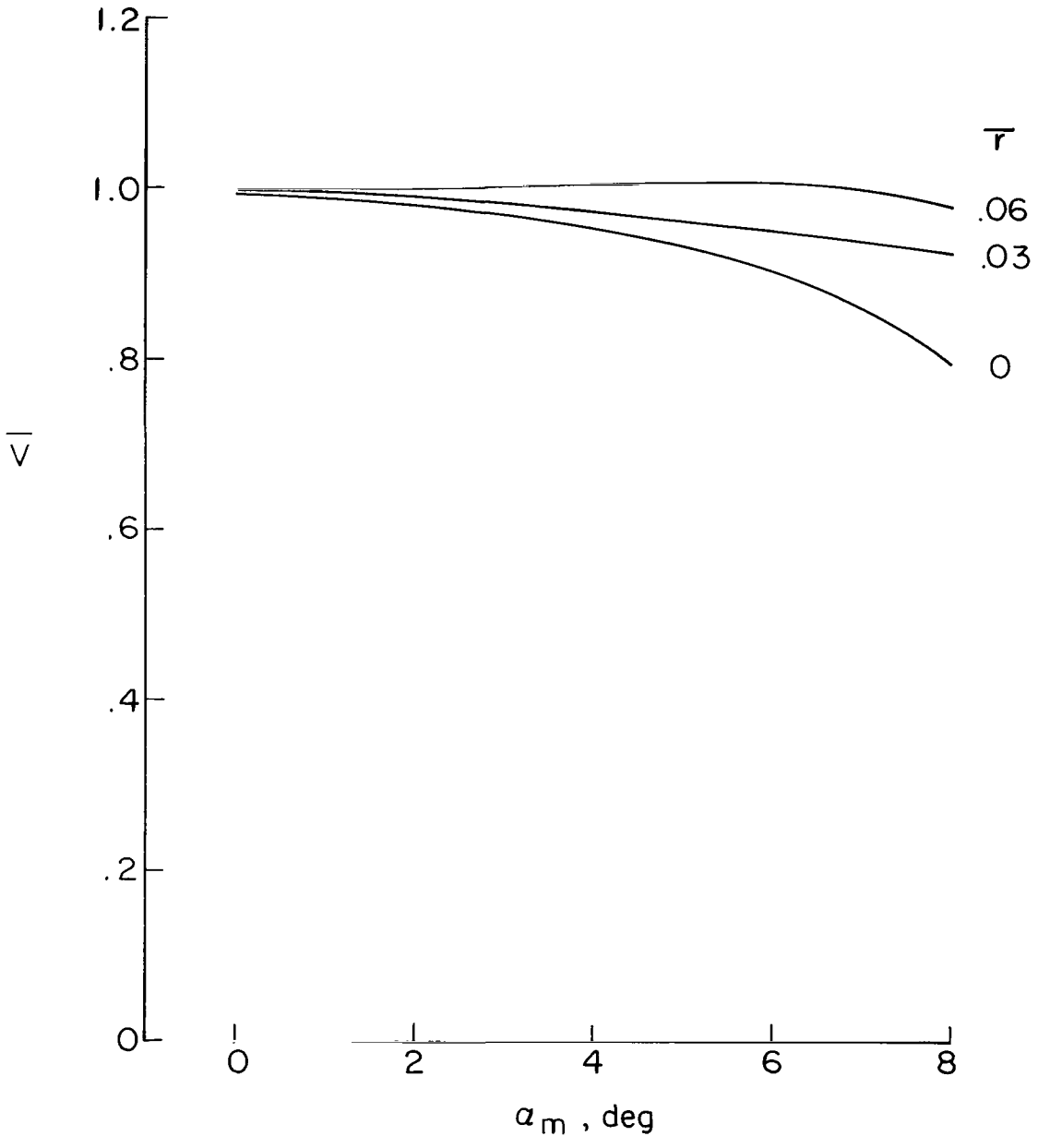

Figure 21.- Effect of mean angle of attack on the quasi-steady flutter speed for sharp and blunt 5^0 double-wedge airfoils at M = 15.3.

NATIONAL AERONAUTICS AND SPACE ADMINISTRATION
WASHINGTON, D. C. 20546

OFFICIAL BUSINESS

FIRST CLASS MAIL

POSTAGE AND FEES PAID
NATIONAL AERONAUTICS AND
SPACE ADMINISTRATION

POSTMASTER: If Undeliverable (Section 158 Postal Manual) Do Not Return

"The aeronautical and space activities of the United States shall be conducted so as to contribute . . . to the expansion of human knowledge of phenomena in the atmosphere and space. The Administration shall provide for the widest practicable and appropriate dissemination of information concerning its activities and the results thereof."

—NATIONAL AERONAUTICS AND SPACE ACT OF 1958

NASA SCIENTIFIC AND TECHNICAL PUBLICATIONS

TECHNICAL REPORTS: Scientific and technical information considered important, complete, and a lasting contribution to existing knowledge.

TECHNICAL NOTES: Information less broad in scope but nevertheless of importance as a contribution to existing knowledge.

TECHNICAL MEMORANDUMS: Information receiving limited distribution because of preliminary data, security classification, or other reasons.

CONTRACTOR REPORTS: Scientific and technical information generated under a NASA contract or grant and considered an important contribution to existing knowledge.

TECHNICAL TRANSLATIONS: Information published in a foreign language considered to merit NASA distribution in English.

SPECIAL PUBLICATIONS: Information derived from or of value to NASA activities. Publications include conference proceedings, monographs, data compilations, handbooks, sourcebooks, and special bibliographies.

TECHNOLOGY UTILIZATION PUBLICATIONS: Information on technology used by NASA that may be of particular interest in commercial and other non-aerospace applications. Publications include Tech Briefs, Technology Utilization Reports and Notes, and Technology Surveys.

Details on the availability of these publications may be obtained from:

SCIENTIFIC AND TECHNICAL INFORMATION DIVISION

NATIONAL AERONAUTICS AND SPACE ADMINISTRATION

Washington, D.C. 20546